Title

Tumor-Associated Carbohydrate Antigen 19-9 (CA 19-9), a Promising Target for Antibody-Based Detection, Diagnosis, and Immunotherapy of Cancer.

Authors

Nakisa, Athar

Sempere, Lorenzo

Chen, Xi

et al.

Publication Date

2024-09-04

DOI

10.1002/cmdc.202400491

Peer reviewed

ChemMedChem

Review
doi.org/10.1002/cmdc.202400491

Chemistry Europe
European Chemical Societies Publishing

www.chemmedchem.org

Tumor-Associated Carbohydrate Antigen 19–9 (CA 19–9), a Promising Target for Antibody-Based Detection, Diagnosis, and Immunotherapy of Cancer

Athar Nakisa,[a, b] Lorenzo F. Sempere,[c] Xi Chen,[d] Linda T. Qu,[e] Daniel Woldring,[b, f] Howard C. Crawford,[g, h] and Xuefei Huang*[a, b, i]

Carbohydrate antigen 19–9 (CA 19–9) also known as sialyl Lewis A is a tetrasaccharide overexpressed on a wide range of cancerous cells. CA 19–9 has been detected at elevated levels in sera of patients with various types of malignancies, most prominently pancreatic ductal adenocarcinoma. After its identification in 1979, multiple studies have highlighted the significant roles of CA 19–9 in cancer progression, including facilitating extravasation and eventually metastases, proliferation of cancer cells, and suppression of the immune system. Therefore, CA 19–9 has been considered an attractive target for cancer diagnosis, prognosis, and therapy. This review discusses the synthesis of CA 19–9 antigen, elicitation of antibodies through vaccination, development of anti-CA 19–9 monoclonal antibodies, and their applications as imaging tracers and therapeutics for a variety of CA 19–9-positive cancer.

Introduction

Glycosylation installs complex glycan moieties as part of glycoproteins and glycolipids on cell surface.[1,2] The glycosylation patterns on cancerous cells can change significantly compared to those on normal counterpart cells, altering multiple cellular signaling events, and facilitating cancer progression.[3–5] These changes result in the formation of tumor-associated carbohydrate antigens (TACAs).[6,7] A representative TACA is sialyl Lewis A (sLe^a) also known as carbohydrate antigen 19–9 (CA 19–9), which is both a local (anchored on cell surface or tumor site) and shed (in systemic circulation) antigen. CA 19–9 is expressed at low levels in normal tissues but overexpressed in cancer cells.[8] Elevated serum levels of CA 19–9 have been detected in a wide range of cancers including pancreatic, biliary, hepatocellular, gastrointestinal, urological, pulmonary, gynecological, thyroid, and salivary gland cancers but most prominently, pancreatic ductal adenocarcinoma (PDAC).[9–17] While the CA 19–9 level in human sera is not reliable for tumor detection,[18] it is the only Food and Drug Administration (FDA)-approved serum biomarker to help manage patients with confirmed PDAC and serially monitor their responses to therapy and disease progression.[9]

CA 19–9 was discovered in 1979 as a tumor antigen due to its recognition by the monoclonal antibody (mAb) 1116NS-19.[19] Many studies have since shown that an increase in the expression of sialylated glycans, such as CA 19–9, promotes tumor metastasis through increased binding of circulating tumor cells to E-selectin on endothelial cells.[20–23] A recent ground-breaking study reported that the expression of CA 19–9 in mice resulted in severe pancreatitis, due to the hyperactivation of epidermal growth factor receptor (EGFR) signaling.[24] Furthermore, CA 19–9 can cooperate with the Kras^{G12D} oncogene to produce aggressive PDAC.[24] Another study demonstrated the immunosuppressive behavior of CA 19–9 for its ability to lead to T-cell apoptosis.[25] Therefore, with its important roles in cancer initiation and progression, CA 19–9 is an attractive target for cancer diagnosis, prognosis, and therapy.

[a] A. Nakisa, X. Huang
Department of Chemistry, Michigan State University, East Lansing, Michigan 48824, United States
E-mail: huangxu2@msu.edu

[b] A. Nakisa, D. Woldring, X. Huang
Institute for Quantitative Health Science and Engineering, Michigan State University, East Lansing, Michigan 48824, United States

[c] L. F. Sempere
Precision Health Program and Department of Radiology, Michigan State University, East Lansing, Michigan 48824, United States

[d] X. Chen
Department of Chemistry, University of California, Davis, California 95616, USA

[e] L. T. Qu
Department of Surgery, Michigan State University, East Lansing, Michigan 48824, United States

[f] D. Woldring
Department of Chemical Engineering and Materials Science, Michigan State University, East Lansing, Michigan 48824, United States

[g] H. C. Crawford
Department of Surgery, Henry Ford Health System, Detroit, Michigan 48202, United States

[h] H. C. Crawford
Department of Pharmacology and Toxicology, Michigan State University, East Lansing, Michigan 48824, United States

[i] X. Huang
Department of Biomedical Engineering, Michigan State University, East Lansing, Michigan 48824, United States

In this review, we first discuss chemical and chemoenzymatic strategies for the synthesis of CA 19–9. This is followed by the development of CA 19–9-based vaccines, anti-CA 19–9 mAbs, and their variants. Subsequently, the applications of anti-CA 19–9 mAbs in imaging and treatment of a variety of CA 19–9-positive malignancies in preclinical studies and clinical trials are discussed to stimulate further studies to address the dire needs in cancer detection and therapy. We will not focus on the applications of CA 19–9 as a biomarker,

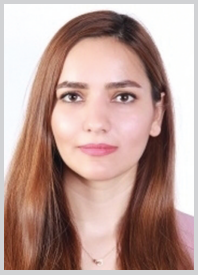

Athar Nakisa is a PhD student at Michigan State University. She received her bachelor's in applied chemistry from the University of Isfahan, Iran, and her master's in organic chemistry from Tarbiat Modares University, Iran. She continued her academic pursuits in the United States, joining Dr. Huang's laboratory at Michigan State University. She has been deeply involved in cancer immunotherapy research. Her work focuses on the development of anti-TACAs (tumor-associated carbohydrate antigens) vaccines and monoclonal antibodies, aiming to advance therapeutic and diagnosis strategies against cancer.

Lorenzo F. Sempere is currently affiliated with the Precision Health Program and Department of Radiology at Michigan State University. He is originally from Elche, a sunny city in southeastern Spain. He was trained with Victor Ambros, microRNA co-discoverer, at Geisel School of Medicine at Dartmouth College. Dr. Sempere initiated his translational cancer research with the support of a Susan G. Komen postdoctoral fellowship and of a Laurie and Paul MacCaskill PanCAN-AACR Career Development award. He has experience and expertise in diverse areas of microRNA research, including evolutionary and developmental biology, molecular and cellular biology, and immunology and cancer biology.

Dr. Xi Chen is a Professor at the Department of Chemistry in University of California (UC), Davis. She received her B.S. degree in Chemistry from Xiamen University in 1994 and her Ph.D. degree in Biological/Organic Chemistry from Wayne State University in 2000. She worked at Neose Technologies, Inc. for two and a half years before joined UC Davis in 2003. Her group is interested in developing efficient chemoenzymatic methods for synthesizing molecules that can help to understand carbohydrate-related biological processes and to develop potential diagnostics and therapeutics.

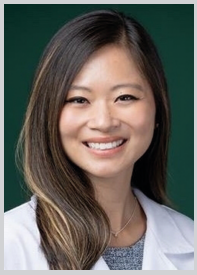

Linda Qu, MD, is a surgical oncologist and assistant professor of surgery in the Department of Surgery at Michigan State University College of Human Medicine. She received her medical degree from Michigan State University College of Human Medicine and completed her general surgery residency at Loyola University Medical Center and fellowship in Complex General Surgical Oncology at the University of Pittsburgh Medical Center. She received a graduate certificate in clinical research from the University of Pittsburgh Institute for Clinical Research Education. She is a health services researcher with interests in cancer outcomes and fragmentation of cancer care.

Daniel Woldring is an assistant professor in MSU's Department of Chemical Engineering and Materials Science and a member of MSU's Institute for Quantitative Health Sciences and Engineering. His research combines high-throughput wet lab methods with machine learning-driven computational tools to engineer high-performance proteins. Research areas being actively pursued in his lab include antibody engineering, membrane transport protein design for drug delivery, antigen recognition in plants, and multi-modal generative AI.

Dr. Howard Crawford has worked in the pancreatic cancer field for the past 25 years, focusing on tumor cell plasticity and inflammation. He is a national and international leader in the pancreatic cancer research field. Dr. Crawford's educational background includes an undergraduate degree from Cornell University, where he graduated Summa Cum Laude; a PhD from the University of Texas Southwestern Medical Center at Dallas; and a postdoctoral fellowship and research faculty appointment at Vanderbilt University.

Xuefei Huang is a MSU Foundation Professor at Michigan State University. He is a full professor jointly appointed in the Departments of Chemistry and Biomedical Engineering, as well as the Chief of the Chemical Biology Division of the Institute for Quantitative Health Science and Engineering. His main research interests are aimed at studying chemistry and biology of carbohydrates. Major focuses of his research include the synthesis of complex carbohydrates and glycoconjugates, the development of novel approaches to boost immune responses against carbohydrate antigens as potential anti-cancer and anti-microbial vaccines, as well as the integration of glyco-science with nanotechnology.

predictor, and promoter of cancer as there are multiple reviews summarizing those areas.[26–31]

Overview of the Structure and Biosynthesis of the CA 19–9 Antigen

Cellular production of CA 19–9 follows a multi-step pathway. CA 19–9 is a branched tetrasaccharide consisting of *N*-acetylneuraminic acid (Neu5Ac), galactose (Gal), fucose (Fuc), and *N*-acetyl glucosamine (GlcNAc) monosaccharides with the sequence of Neu5Acα2-3 Galβ1-3(Fucα1-4)GlcNAcβ1- covalently linked to glycoproteins[32] or glycolipids[33] (Compound **1**, Figure 1a). In nature, CA 19–9 is biosynthesized by the transfer of Neu5Ac to the 3-*O* of the terminal Gal at the non-reducing end in type I *N*-acetyllactosamine (type I LacNAc, Galβ1-3GlcNAc) by sialyltransferase ST3 Gal III, which is followed by α1,4 fucosylation of the GlcNAc in the resulting molecule by the fucosyltransferase 3 (FUT3) (Figure 1b).[34] After recognition of the importance of CA 19–9 as a potential target in cancer therapy and the challenges in isolating sufficient quantities of it from natural sources, synthesis has become the preferred method to prepare CA 19–9 to enable biological investigations.

Chemical Synthesis of the CA 19–9 Antigen

While the chemical synthesis of a CA 19–9 analog dated back to 1994 by the Hasegawa group,[35] the first total synthesis of CA 19–9 was reported in 2000 by Kunz and coworkers.[36] They designed a protected CA 19–9 tetrasaccharide **2** bearing an azido group at the reducing end to facilitate the conjugation of the carbohydrate to an asparagine residue in peptides (Scheme 1a).[36] This synthesis strategy started from the glycosylation of *N*-acetyl and 4,6-*O*-benzylidine protected azido β-glucosamine **3** by 6-*O*-benzyl protected α-galactosyl bromide **4** to yield the azido type I LacNAc **5**. After protective group manipulation, the resulting disaccharide was fucosylated using *O*-benzylated ethylthio-fucoside **6** activated by copper(II)bromide and tetrabutylammonium bromide under the *in situ* anomerization condition to form the α1-4-fucosyl linkage (Lewis A or Le^a trisaccharide **7**). The *O*-acetyl moieties of **7** were removed and the resulting triol was glycosylated by the phenylthioglycoside of protected *N*-acetyl-neuraminic acid methyl ester donor **8** to form **2** in a modest yield of 44% even with 2.7 eq of the donor, which was subsequently deprotected for conjugation with an aspartic acid to form an *N*-linked asparagine.

The second reported chemical synthesis of CA 19–9 as pentenyl glycoside of CA 19–9 hexasaccharide **9** was by the Optimer Pharmaceuticals to facilitate their vaccine studies.[37] While many of the synthesis details were not published, the synthetic route was based on the glycosylation of Neu5Ac-Gal disaccharide donor **10** with a glucosamine acceptor **11** followed by fucosylation (Scheme 1b). In 2023, in their quest for a CA 19–9 based vaccine, Huang group reported the chemical synthesis of CA 19–9 tetrasaccharide **13** (Scheme 1c).[38] To overcome the low yields in the sialylation reaction, rather than the late stage sialylation of the Le^a trisaccharide shown in Scheme 1a, the Huang group performed early sialylation in the synthesis. A new sialyl donor **14** bearing the trifluoroacetyl (TFA) group as the *N*-protective group and *N*-phenyl trifluoroacetimidate as the anomeric leaving group was designed. Selective activation of **14** over thiogalactosyl acceptor **15** led to the desired disaccharide **16** with the α2-3 sialyl linkage in 75% yield. Subsequent protective group manipulation followed by glycosylation with glucosamine acceptor **17** and fucosylation with **18** resulted in tetrasaccharide **19**, which was subsequently deprotected to obtain CA 19–9 tetrasaccharide **13** bearing an amino propyl linker at the reducing end ready for conjugation. Recently, Yang and coworkers reported a new chemical synthesis of CA 19–9 tetrasaccharide **13** (Scheme 1d).[39] They discovered that sialylation of Le^a trisaccharide **20** by the sialyl donor **21** was not successful. Interestingly, removal of the 4′-benzyl (Bn) group from **20** (Le^a triol **22**) led to successful glycosylation by donor **21** in 75% yield presumably due to the reduced steric hinderance of the triol acceptor **22**. Subsequent deprotection of the resulting tetrasaccharide **23** produced CA 19–9 tetrasaccharide **13**.

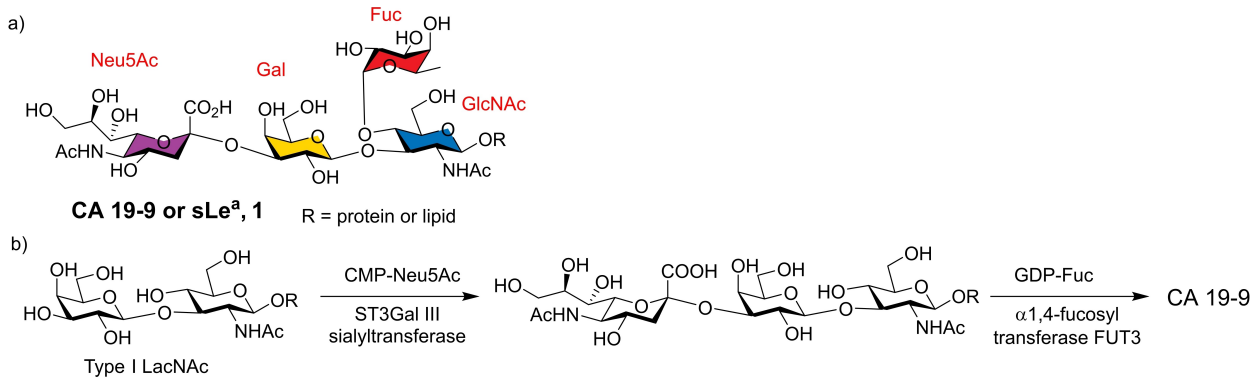

Figure 1. a) The structure of CA 19–9 tetrasaccharide epitope; b) the biosynthetic process and enzymes involved for CA 19–9.

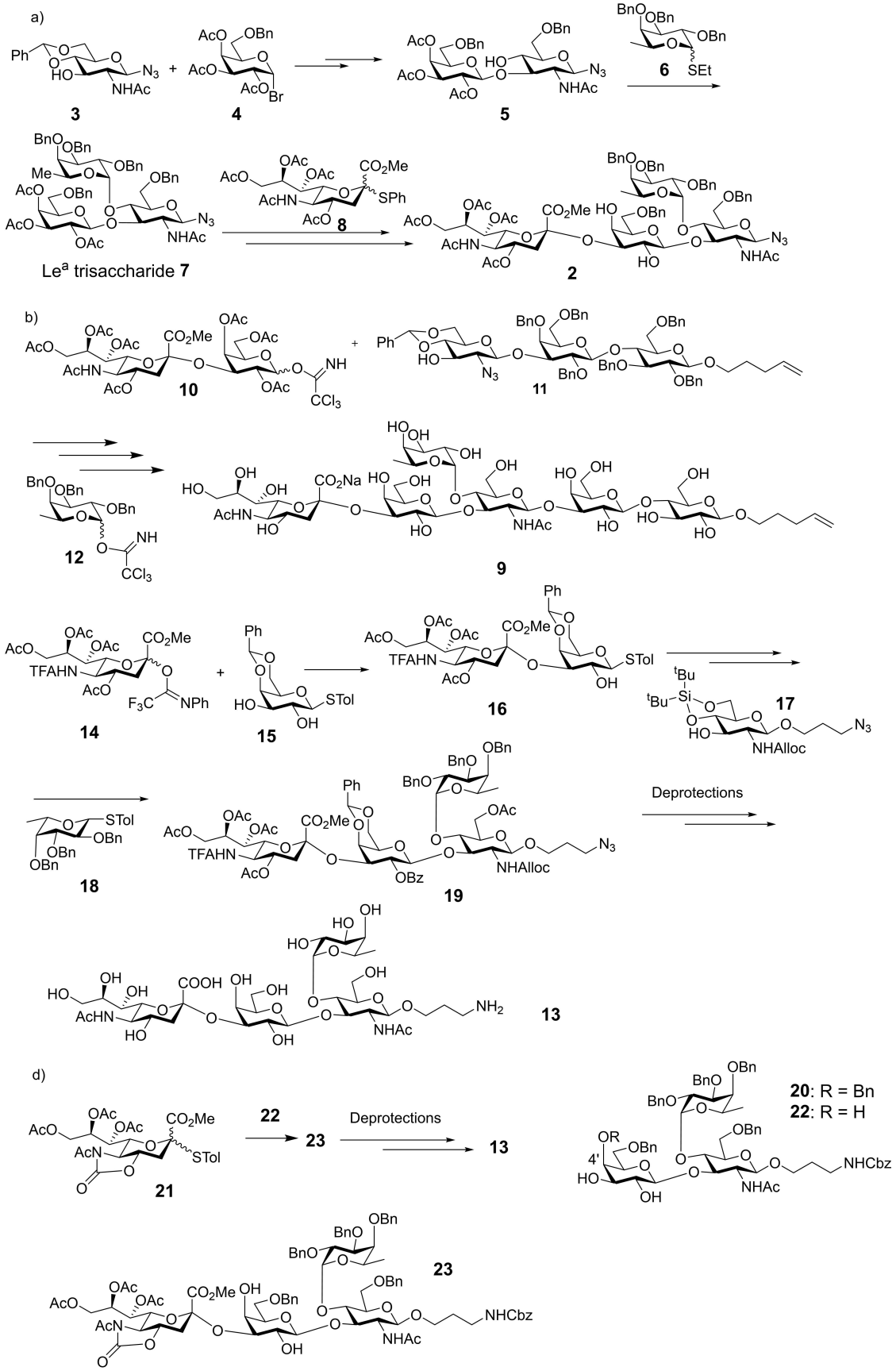

Scheme 1. Chemical synthesis pathways of CA 19–9. Syntheses of a) protected CA 19–9 tetrasaccharide **2**; b) pentenyl CA 19–9 hexasaccharide **9**; c) CA 19–9 tetrasaccharide **13** with an amino propyl linker at the reducing end; and d) a second synthesis of CA 19–9 tetrasaccharide **13.**

Chemoenzymatic Synthesis

As chemical synthesis of CA 19–9 requires multiple steps of protection and deprotection, chemoenzymatic synthesis presents an attractive alternative to enhance the overall synthetic efficiency. Inspired by biosynthesis of CA 19–9, various enzymes have been explored to facilitate its assembly. Multiple α2-3-sialyltransferases have been examined such as EC 2.4.99.5 purified from rat liver,[40] EC 2.4.99.4 from porcine submaxillary glands,[41] and recombinant enzymes.[42] The α1-4-fucosylation of the sialylated type I LacNAc has been achieved by human-milk α(l-3/4)-fucosyltransferase using guanosine 5′-diphosphate-fucose (GDP-Fuc) as the donor.[41] Baisch et. al. reported the synthesis of various CA 19–9 analogs by taking advantage of the substrate promiscuity of a recombinant fucosyl-transferase III tolerating non-natural GDP donors as well as a wide range of non-reducing C-4 amide substituted sialylated type I LacNAc as acceptor.[43]

Chemoenzymatic synthesis of CA 19–9 was reported for the first time by Kiso and coworkers using a sialidase from *Salmonella* typhimurium LT2 (Scheme 2a).[44] They used chemically synthesized *p*-nitrophenyl sialyl glycoside **24** as the glycosyl donor and Le^a trisaccharide **25** as the glycosyl acceptor. While the sialidase installed the α2-3 sialyl linkage highly regioselectively, the reaction yield was low at 12%. In 2018, a highly efficient chemoenzymatic synthesis of a library of CA 19–9 was reported by the Chen group.[45] The process started with the gram-scale chemical synthesis of azido propyl functionalized GlcNAc **27** from GlcNAc followed by enzymatic synthesis of disaccharide Galβ1-3GlcNAcβProN_3 **28** using a one-pot multi-enzyme (OPME) galactosylation strategy by incubating chemically synthesized GlcNAcProN_3 **27** with galactose, and adenosine 5′-triphosphate (ATP) in the presence of recombinant bacterial enzymes *Streptococcus pneumoniae* galactokinase (SpGalK) and *Bifidobacterium infantis* D-galactosyl-β1-3-*N*-acetyl-D-hexosamine phosphorylase (BiGalHexNAcP) (Scheme 2b).[46] Unlike a galactosyl transferase requiring the uridine 5′-diphosphate-galactose (UDP-Gal) as the donor, the BiGalHexNAcP can efficiently transfer the Gal unit from Gal-1-phosphate leading to the type I LacNAc **28** in an excellent yield of 90%. Interestingly, rather than following the biosynthetic route of CA 19–9, they performed fucosylation first by incubating disaccharide **28**, L-fucose, ATP, and GTP with recombinant *Helicobacter pylori* α1-3/4-fucosyltransferase (Hp3/4FT), *Bacteroides fragilis* enzyme with both L-fucokinase and GDP-Fuc pyrophosphorylase activities (BfFKP), and *Pasteurella multocida* inorganic pyrophosphatase (PmPpA) as a OPME fucosylation system, which formed Le^a trisaccharide **29** in 91% yield. Subsequently, CA 19–9 **30** was prepared by incubating Le^a trisaccharide **29** with *N*-acetyl mannosamine (ManNAc) in an OPME sialylation system including *Pasteurella multocida* sialic acid aldolase (PmNanA) for *in situ* synthesis of Neu5Ac, *Neisseria meningitidis* CMP-sialic acid synthetase (NmCSS) for *in situ* formation of the cytidine-5′-monophospho-*N*-acetylneuraminic acid (CMP-Neu5Ac) donor and *Pasteurella multocida* α2-3-sialyltransferase 1 M144D mutant (PmST1 M144D).[47] PmST1 M144D was able to install Neu5Ac onto the Le^a trisaccharide **29**. This route represents an efficient synthesis of CA 19–9 with gram quantity preparation of Le^a trisaccharide and the production of multiple CA 19–9 analogs bearing diverse modifications on the terminal sialic acid component. In an alternative chemoenzymatic synthesis, the Yang group sialylated the type I LacNAc **31** first with

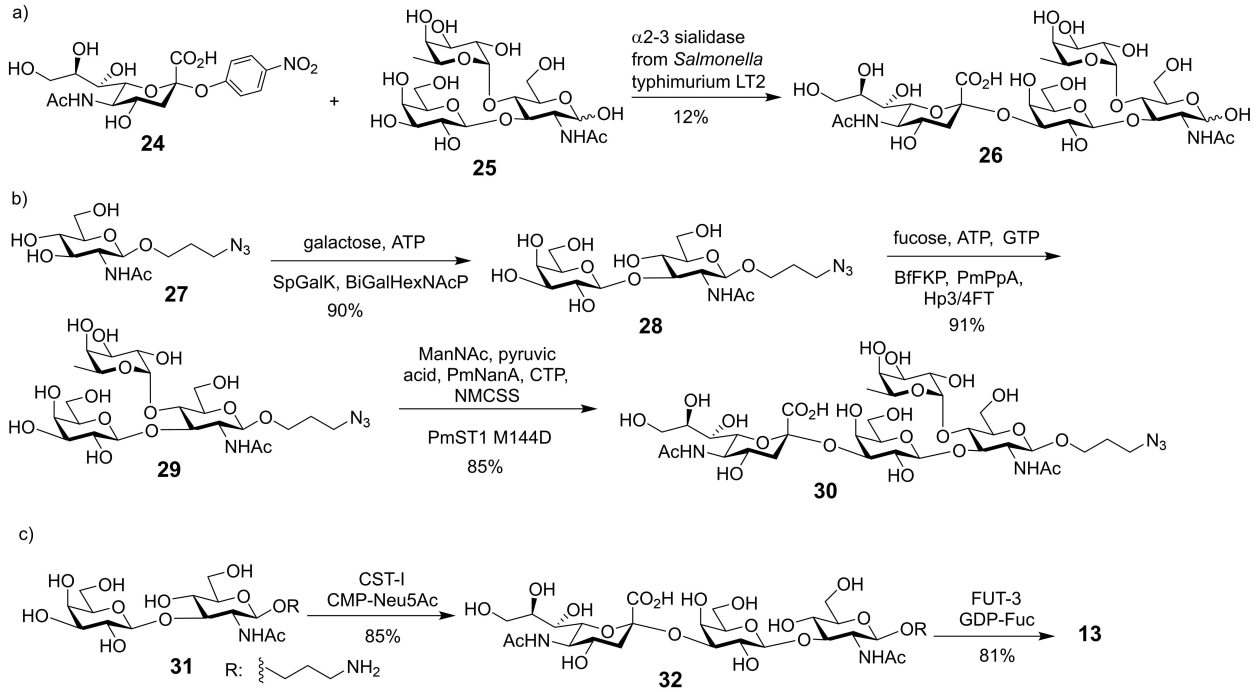

Scheme 2. a) Sialidase catalyzed synthesis of CA 19–9 **26**; b) one pot multi-enzyme (OPME) synthesis of CA 19–9 **30**; and c) chemoenzymatic enzymatic synthesis of CA 19–9 **13**.

Campylobacter jejuni α2,3-sialyltransferase I (Cst-I) (Scheme 2c).[39] The resulting trisaccharide **32** was fucosylated with FUT3 leading to CA 19–9 tetrasaccharide **13** demonstrating that enzymatic sialylation and fucosylation do not interfere with each other.

Development of CA 19–9 Based Cancer Vaccines

Cancer vaccines are a form of immunotherapy, which can induce immune responses in vaccinated subjects to recognize and eliminate cancer cells potentially with few side effects.[48–50] As a result, cancer vaccines can complement current chemo-, radiation-, and immune therapies. With their high levels of expression on many types of tumors, TACAs are attractive antigenic targets for vaccine development.[6,7] However, administration of TACAs alone can only generate low levels of IgM antibodies, not capable of providing long-term protection against tumor development (Figure 2a). This is due to the weak immunogenicity of TACAs and their inability to activate helper T (T_h) cells or $CD4^+$ T cells. To overcome this challenge, TACAs need to be conjugated to immunogenic carriers to boost the immune responses. After binding of antigens (TACAs conjugated on protein carriers) to the B cell receptor (BCR), the conjugate is endocytosed and digested inside the cells. The peptide epitopes released are then presented to $CD4^+$ T_h cells via MHC II molecules on B cell surface. Binding of T cell receptors (TCRs) on T_h cells to peptide antigens presented on MHC II molecules results in the activation of T_h cells with the subsequent binding of CD40 on B cells with CD40 ligand (CD40 L) on T_h cells. These interactions result in the release of cytokines such as IL-4 and IL-21 from T_h cells, which can further activate B cells leading to antibody isotype switching to IgG. As a result, B cells can differentiate to become plasma cells for IgG antibody production and memory cells[51] (Figure 2b).

The first CA 19–9-based vaccine was reported in 2009.[37] The pentenyl glycoside of CA 19–9 compound **9** was subjected to ozonolysis to introduce an aldehyde at its reducing end, which was subsequently coupled to a thiolated protein carrier, Keyhole Limpet Hemocyanin (KLH) (Scheme 3a). Mice were immunized with the resulting KLH-CA 19–9 conjugate four times together with GPI-0100, a semi-synthetic mix of saponin fractions as the adjuvant. Analysis of the post-immune sera indicated that administration of CA 19–9 or admixture of CA 19–9 with KLH failed to produce any anti-CA 19–9 IgG or IgM antibodies in most mice, confirming the low immunogenicity of CA 19–9 as a standalone antigen. In contrast, mice vaccinated with the KLH-CA 19–9 conjugate produced IgG antibodies against CA 19–9, which were able to bind to CA 19–9-positive ovarian cancer cells SW626. Inclusion of GPI-0100 adjuvant in vaccination greatly improved the anti-CA 19–9 antibody responses. The antibodies could kill tumor cells via complement-dependent cytotoxicity, highlighting the potential of the vaccine. A human clinical trial confirmed the safety and immunogenicity of the KLH-CA 19–9 conjugate. However, to date, no tumor protection efficacy results have been reported in humans or animal models for this construct.[52]

To enhance the immune responses against CA 19–9, alternative carriers such as virus-like particles (VLPs) have been investigated. VLPs typically consist of repeating units, arranged

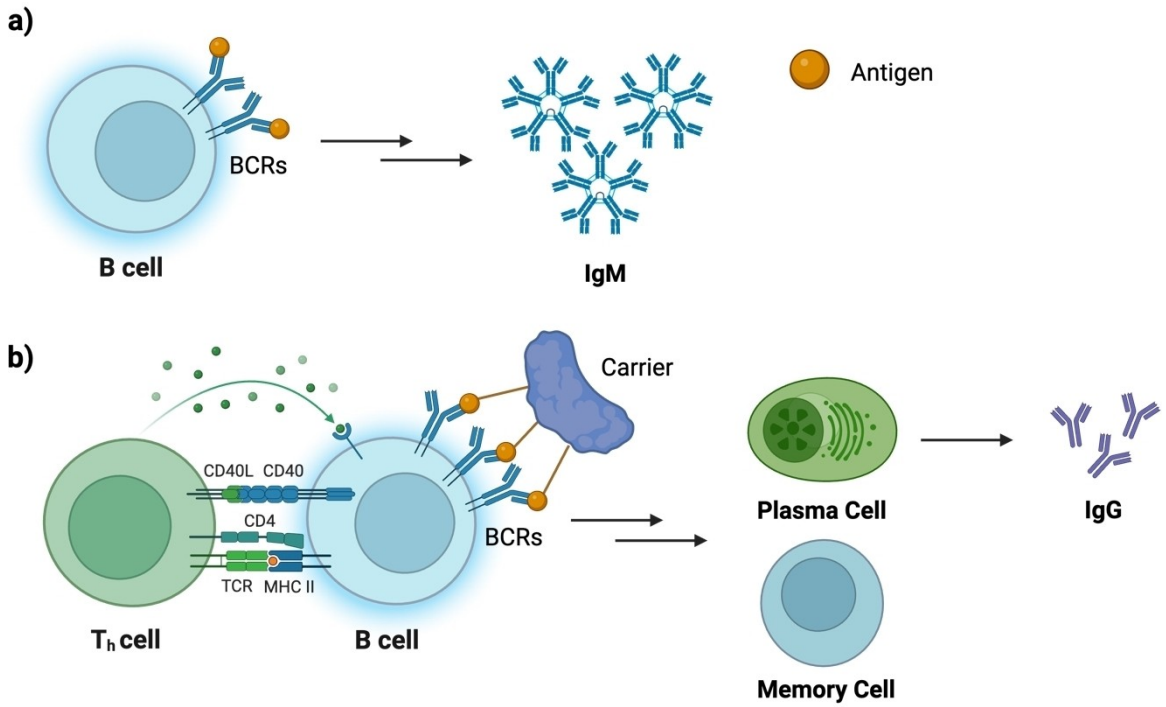

Figure 2. Activation of B cells a) in the absence of Th cell binding through low-affinity binding of TACA to B cell receptors to secret IgM, and b) in the presence of Th cell binding through high-affinity cross-binding of TACA to B cell receptors to secret IgG. (Created with BioRender.com).

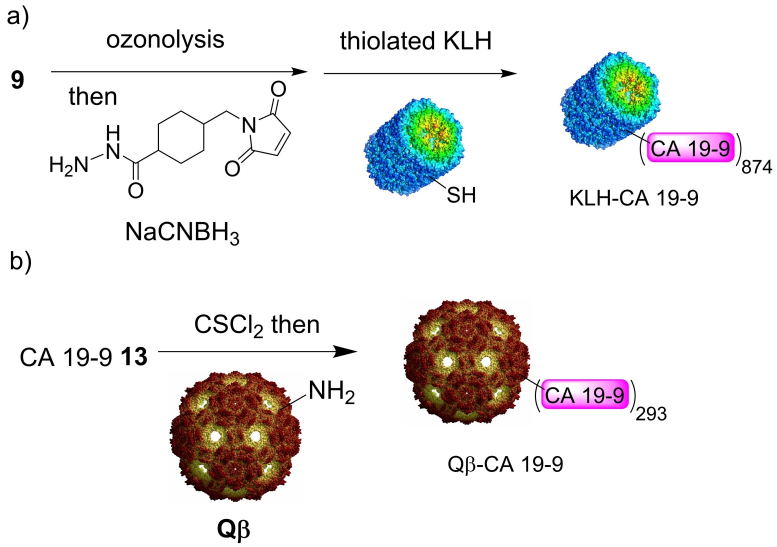

Scheme 3. Synthesis of a) a KLH-CA 19–9 conjugate from the allyl glycoside derivative of CA 19–9 **9**; b) the Qβ-CA 19–9 conjugate from the aminated CA19-9 **13**.

in a well-ordered manner in 3D space. Their 3D orientation allows them to present antigens in an organized manner to B-cell receptors (BCRs), leading to enhanced multivalent affinity binding and more effective B-cell activation.[53] Huang group in their recent study[38] utilized a powerful VLP, mutant bacteriophage Qβ[54] as the carrier for CA 19–9 vaccine development. Following the synthesis of CA 19–9 **13**, the reducing end amine group was converted to isothiocyanate, which reacted with Qβ installing an average of 293 copies of glycan per Qβ particle (Scheme 3b). For comparison, the corresponding KLH-CA 19–9 conjugate was prepared using the same chemistry with an average of 399 copies of antigen per KLH. Mice were immunized with Qβ-CA 19–9 and KLH-CA 19–9 conjugates respectively three times two weeks apart. As analyzed by enzyme-linked immunosorbent assay (ELISA), while mice immunized with KLH-CA 19–9 produced anti-CA 19–9 IgG antibodies, the Qβ-CA 19–9 group exhibited several orders of magnitude higher titers of long-lasting IgG in comparison, highlighting the superior immunogenicity of Qβ carrier (Figure 3a). In addition, vaccination with the admixture of Qβ and CA 19–9 was ineffective in inducing anti-CA 19–9 IgG antibodies, confirming the importance of conjugating Qβ with CA 19–9. The antibodies induced by Qβ-CA 19–9 bound well to CA 19–9-positive tumor cells and killed the cells via complement mediated cytotoxicity. Vaccination of mice with Qβ-CA 19–9 significantly reduced the number of tumor foci in a cancer metastasis to lung model (Figures 3b–d), and the antibodies could recognize a wide range of human PDAC tissues in a microarray study, highlighting the translational potential of the Qβ-CA 19–9 conjugate.

Anti-CA 19–9 Monoclonal Antibody Development

In parallel to vaccines, monoclonal antibodies (mAbs) specific against CA 19–9 have been developed, which are highly useful tools for tumor detection and treatment. mAbs are Y-shaped macromolecules (Figure 4) produced by identical clones of B lymphocytes against a specific antigen. They have revolutionized the biomedical field due to their high affinity and specificity. Typical mAbs are homodimers with each monomer consisting of a heavy chain and a light chain. The antigen-binding or variable regions (Fab) are located on the arms and include *N*-terminal domains of both the heavy and the light chains responsible for antigen binding through the complementary-determining regions (CDRs). The C-terminal domains of the heavy chain are the stems of the mAb, commonly referred to as fragment crystallizable region (Fc region), which is constant among a subtype of antibody. For example, for mouse IgG antibody, various subtypes are defined by the Fc domain to be IgG1, IgG2a, IgG2b, IgG2c, and IgG3. Fc interacts with other components of the immune system, such as cell receptors and proteins, which help in recruiting immune cells and other molecules to destroy the antigen bearing target once it is bound by the mAb (Figure 4).

mAbs have become a major category of new drugs developed in recent years. In 2018, eight of the top ten best-selling drugs globally were mAbs, with an overall market valued around $115 billion.[55] mAbs have been applied in a broad range of diseases for both therapy and diagnosis. They can be utilized as monotherapy, in combination with other therapies, a delivery system for highly toxic payloads to the target site (antibody drug conjugates or ADCs), or agents to facilitate non-invasive imaging.

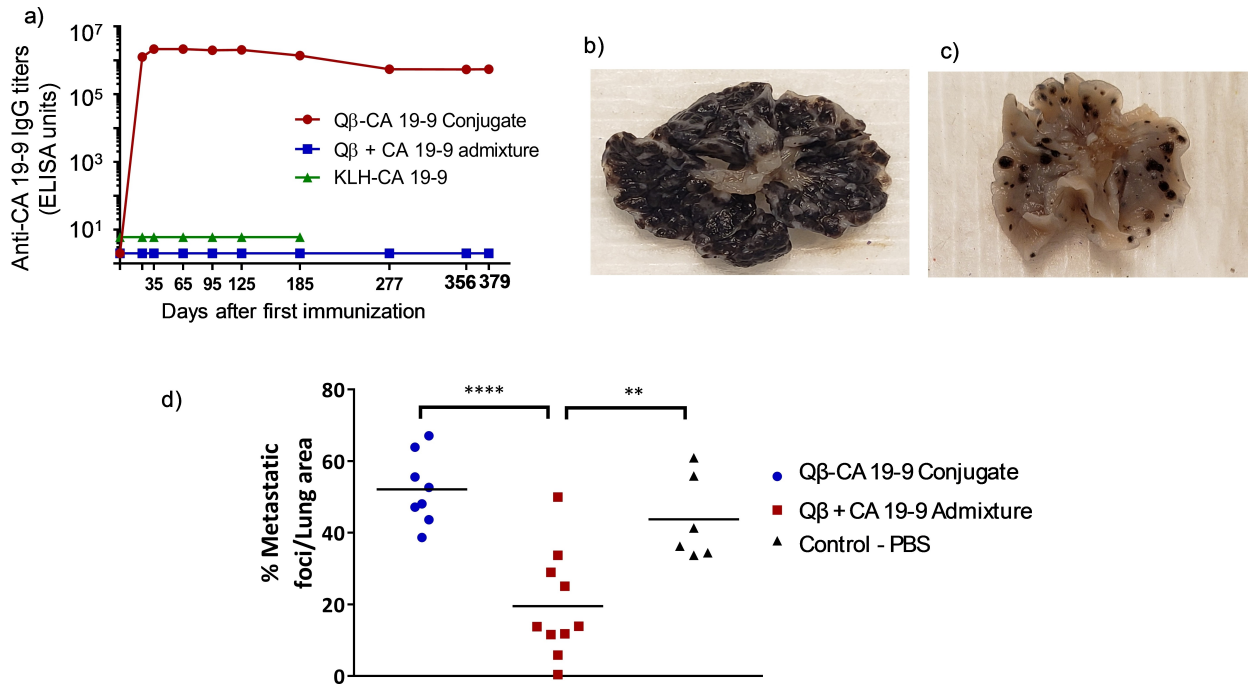

Figure 3. a) Immunization with Qβ-CA 19–9 conjugate elicited high levels and long last IgG antibodies against CA 19–9 compared to mice receiving the KLH-CA 19–9 conjugate or the admixture of Qβ and CA 19–9; b) A representative image of a lung of mouse immunized with PBS mock control in a tumor metastasis model. The black color was due to tumor growth; c) A representative image of a lung of mouse immunized with Qβ-CA 19–9 conjugate in a tumor metastasis model with B16-FUT3 cells; d) Quantification of the tumor areas in lungs of mice immunized with Qβ-CA 19–9 conjugate, admixture of Qβ and CA 19–9, and PBS mock control. Immunization with Qβ-CA 19–9 significantly reduced the tumor areas in the lungs.

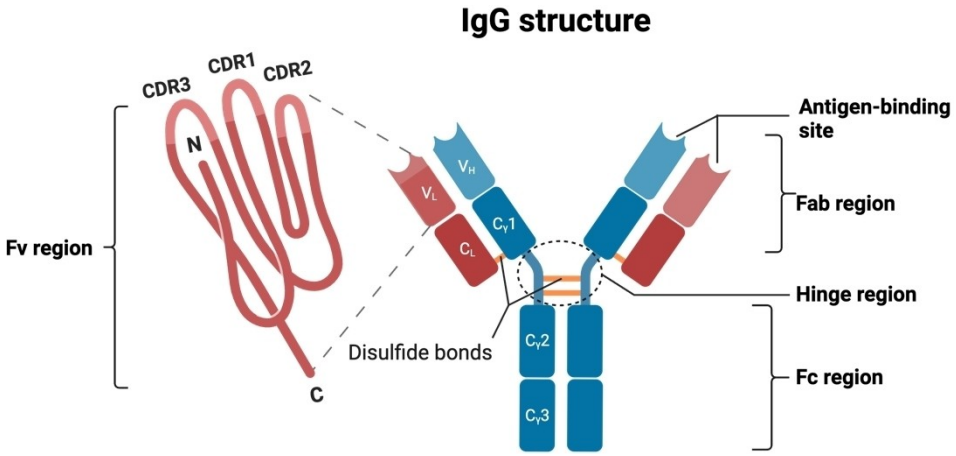

Figure 4. Structure of an IgG antibody (Created with BioRender.com).
C = constant, V = variable, L = light, H = heavy.

Advances in Antibody Engineering and Development Techniques

The fast pace of mAb development is due to the outstanding progress in antibody engineering including humanization of mAbs, phage display, single B cell antibody technology, and affinity maturation.[56] These have overcome some of the main limitations of mAb development, such as toxicity, low efficacy, and high cost.[57] Hybridoma is the first and the most common technology in mAb development. In this technique, B lymphocytes are isolated from humans or animals that are immunized with a specific antigen and then fused with immortal myeloma cells to produce hybridoma (Figure 5). The resulting mixture is cultured in a selective media to grow only hybridoma cells that are then screened to select the clone of mAb with the highest affinities towards the antigen. This is the main technology applied to develop many anti-CA 19–9 mAbs,[58] and some of the reported anti-CA 19–9 mAbs are summarized in Table 1.

The first reported anti-CA 19–9 mAb (1116NS-19) was discovered by Koprowski and coworkers in 1979 while they were developing colorectal carcinoma-specific antibodies by hybridoma technology.[19] Mice were immunized with colorectal

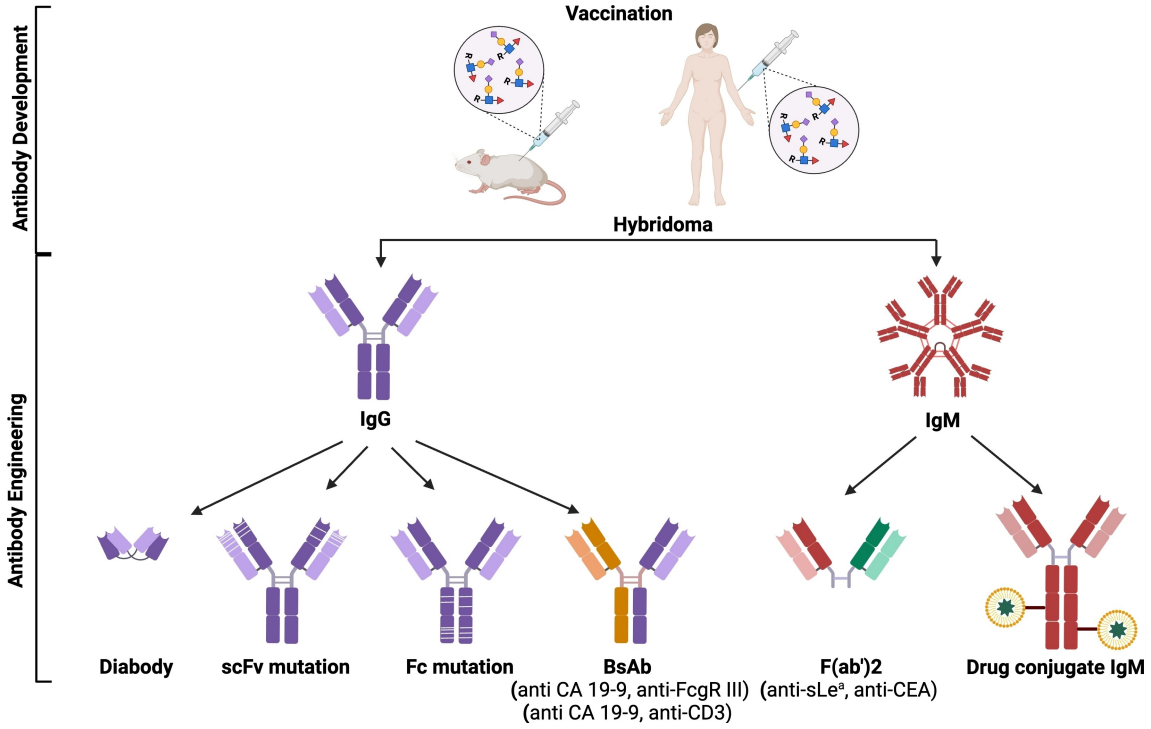

Figure 5. Anti-CA 19–9 antibodies development and engineering (Created with BioRender.com).

Table 1. A summary of the reported anti-CA 19–9 mAbs.

No	Clone name	Development approach	Isotypes	K_D (nM)	Host species	Immunogen	Year
1	1116NS-19 or 1116NS-19-9	Hybridoma	IgG1	30[62] 42[42]	Mouse	SW 1116	1979
2	CO 29.11	Hybridoma	IgG1	20[62]	Mouse		1985
3	SA23.2	Hybridoma	IgM		Mouse	Purified glycolipid CA 19–9	1999
4	LC44	Hybridoma	IgG3		Mouse	CA 19–9	2006
5	5B1	Hybridoma	IgG1	0.14[64]	Human	KLH-sLe^a	2011
6	7E3	Hybridoma	IgM	0.04[64]	Human	KLH-sLe^a	2011

cancer cell line SW 1116 and their splenocytes were isolated and fused with myeloma cell line P3X63 Ag8. Nineteen out of the 76 isolated hybridoma, including 1116NS-19, showed binding to human tumors, but not normal cell lines. Later, they discovered that binding of 1116NS-19 to SW 1116 cells was abolished upon treatment of the cells with a neuraminidase, but binding to SW 1116 cells treated with the protease ficin was unaffected suggesting the antigen might be a sialylated glycolipid.[59] Therefore, total cell lipids were extracted and the antigen was identified as a monosialylganglioside. The binding ganglioside was then purified and characterized through enzymatic/chemical degradation followed by mass spectrometry analysis to be CA 19–9 containing ganglioside.[33] The binding of 1116NS-19 antibody to SW 1116 cells was found to be inhibited by sera of human patients with colorectal adenocarcinoma, gastric and pancreatic carcinoma but not by sera of normal individuals or individuals with other cancer types, showing the high level of antigen in sera of patients with gastrointestinal carcinomas.[60] Interestingly, through analysis of antigens in different fractions of serum, it was found that although CA 19–9 had been detected as monosialylganglioside in colorectal cancer cells, the antigen is mainly expressed on mucin glycoproteins in colon cancer patient sera.[61] CA 19–9 was also found in low concentrations in mucins secreted by normal cells at pancreas ducts, salivary glands, and bronchial epithelium.[61] The binding of 1116NS-19 to CA 19–9 is quite specific with no binding observed for the Le^a trisaccharide suggesting the sialic acid unit is a critical part of the epitope.

Another anti-CA 19–9 mAb called CO 29.11 was developed by Herlyn et. al. using the hybridoma technology.[62] Similar to 1116NS-19, CO 29.11 is also an IgG1 and recognizes only cells of gastrointestinal tumors such as gastric, pancreatic, and colorectal carcinomas. In comparison to 1116NS-19, CO 29.11 has a slightly higher affinity towards CA 19–9 (K_a for CO 29.11 is $5\times10^7\ M^{-1}$ and for 1116NS-19 is $3\times10^7\ M^{-1}$),[31] and higher sensitivity for detection of early cancer and recurrence. However, CO 29.11 is not specific to CA 19–9 with some weak

binding to Le^a trisaccharide indicating that the epitopes for CO 29.11 and 1116NS-19 are different.

Immune suppression by tumor cells is one of the major challenges in tumor immunotherapy. Some tumor antigens such as MUC1 may cause T cell apoptosis, dampening the anti-tumor immunity.[63] Li et. al. reported that CA 19–9 as part of a mucin antigen can lead to T-cell apoptosis.[25] To inhibit the T-cell suppression activity of CA 19–9, they produced LC44 as an antagonistic mAb using the hybridoma technology. Applying LC44 to the mixture of human T-cells and CA 19–9, which resulted in the production of antibody-antigen immunocomplex, improved T-cell proliferation *in vitro*. LC44 also exhibited effective complement dependent cytotoxicity (CDC) activity against SW 1116 cells.[25]

A drawback of obtaining mAbs from mice is that mouse antibodies induce immune responses in humans, which is detrimental for clinical studies and requires an extra step to humanize the antibody. To overcome this limitation, Sawada et. al. reported two fully human anti-CA 19–9 mAbs, i.e., 5B1 and 7E3.[64] These two mAbs were obtained by the fusion of P3X63 Ag8.653 myeloma cells with blood lymphocytes from two breast cancer patients immunized by the KLH-CA 19–9 vaccine. Variable regions of these two antibodies were detected and cloned in IgG for 5B1 and IgM for 7E3 to produce recombinant antibodies using Chinese hamster ovary (CHO) cells. Both antibodies showed high affinity towards a polyvalent CA 19–9 construct as measured by surface plasmon resonance (SPR) with K_D values of 0.14 nM for 5B1 and 0.04 nM for 7E3. They also exhibited high specificity towards CA 19–9 by glycan microarray studies showing no binding to structurally similar carbohydrates including Le^a and sLe^x, as well as ganglioside glycans GD2, GD3, fucosyl-GM1, GM2, and GM3. 5B1 could kill CA 19–9-positive lung cancer cells DMS-79 via both CDC and antibody dependent cellular cytotoxicity (ADCC) mechanisms using human peripheral blood mononuclear cells (PMBC) as the effector cells. To better understand how the CA 19–9 antigen is recognized by mAbs, high resolution co-crystal structures of CA 19–9 with 5B1 and 1116NS-19 respectively were obtained by X-ray crystallography.[65] While little structural changes were observed for 5B1 in the CA 19–9 complex vs the apo structure, 1116NS-19 underwent significant conformational changes to bind to CA 19–9, suggesting an induced-fit binding mechanism. Interestingly, despite the different binding mechanisms and primary sequences of the two mAbs, CA 19–9 exhibited an essentially identical extended low-energy conformational state in both co-crystal structures. These results indicate that this stable conformer selects the antibodies.

Engineered Anti-CA 19–9 Antibodies

Binding affinity and specificity of an antibody toward an antigen are critical criteria in mAb development. Naturally existing antibodies can be further evolved *in vitro* to enhance their properties. In 2020, Amon et. al. took advantage of the yeast surface display (YSD) platform to evolve a library of anti-CA 19–9 antibodies.[66] A plasmid containing the sequence for single chain fragment variable region (scFv) of variable heavy chain (V_H) and variable light chain (V_L) of 1116-NS-19-9 antibody connected by a $(G_4S)_3$ linker was constructed. Using error-prone PCR with 1–2 mutations/scFv, a library of RA9-mutants-scFv was generated, which was then cloned into pETCON2 plasmid and transformed into yeast cells. The binding of the surface-expressed scFv with the CA 19–9 antigen was evaluated by fluorescence-activated cell sorting (FACS) and the high affinity clones were enriched by three rounds of panning using FACS sorting. The evolved scFvs were purified, sequenced, and cloned to express full-length recombinant IgGs. The evolved antibodies were highly selective toward CA 19–9 binding, as several structurally similar glycans including sLe^x, Le^a, Le^y, and Le^x only exhibited weak binding ($<5\%$). sLe^x contains the same four monosaccharides as CA 19–9. Its low binding to the antibodies suggested that the 3D arrangement of the monosaccharides is critical. The low binding of the antibodies to Le^a confirms the crucial role of sialic acid as the epitope. Biolayer interferometry[42] measurements were performed to quantify the binding affinities, which demonstrated that the mutated antibodies have higher CA 19–9 affinities ($K_D = 9–37$ nM) in comparison to the native antibody ($K_D = 42$ nM). A newly evolved antibody RA9-23 could recognize CA 19–9-positive cell lines (WiDr, Capan-2, BxPC-3), but not CA 19–9-negative cell lines (MCF-7, MDA-MB-231). RA9-23 had a stronger binding to both WiDr and Capan-2 cell lines compared to the native 1116-NS-19-9 antibody. RA9-23 also showed higher CDC activities against both WiDr and Capan-2 cell lines.

The activities of antibodies in cancer therapy require recognition of antigen on cancerous cells surface through the Fab region. Upon binding, antibodies can activate effector functions such as ADCC and antibody-dependent cellular phagocytosis (ADCP) by the Fc domain. An important factor in determining the ability of IgG Fc dependent antibody-related cytotoxicity is the ratio of binding to activating versus inhibitory (A/I) Fcγ receptors (FcγRs), which is determined as 0.1 for IgG1 (the lowest) and 70 for IgG2a (the highest).[67] The Ravetch group reported innovative studies to engineer the Fc domains of two anti-CA 19–9 mAbs, i.e., 5B1 and 7E3.[68] Three mutations (G236 A/A330 L/I332E, termed GAALIE) were introduced into the Fc domain of the mAbs respectively. These mutations improved the binding of the Fc to activating versus inhibitory FcγRs and increased the A/I ratios for both 5B1 and 7E3. Subsequently, a lung metastasis model was established by intravenously injecting CA 19–9 expressing mouse melanoma cell B16-FUT3 on day 0 to FcγR-humanized C57BL/6 immunocompetent mice. Engineered 5B1-GAALIE, 7E3-GAALIE and isotype matched human IgG1 were administered on days 1, 4, 7, and 11 at 100 μg per injection. The Fc variants of 5B1 and 7E3 were both able to significantly inhibit lung colonization of tumor cells. The higher potency was attributed to the enhancement of binding of new anti-CA 19–9 antibodies to activating human FcγRs, hFcγRIIA and hFcγRIIIA, as well as decreased binding to the inhibitory receptor, hFcγRIIB.

Bispecific Antibodies and Cellular Therapy

Typical mAbs have two identical Fabs (Figure 4) that allow the antibody to bind two of the same antigens. More recently, bispecific antibodies have been engineered containing two heterologous Fabs with different binding specificities referred to as bispecific antibodies. Bispecific antibodies can simultaneously engage two different antigens, which can significantly broaden the utilities of the antibodies (Figure 5).

One of the challenges in applying mouse antibody for clinical cancer therapy is the failure to activate human effector cells by these murine mAbs, which results in inefficient immune response to lyse cancerous cells. This is because the Fc domain of mouse antibodies cannot be recognized well by FcγRs on the surface of human effector cells. To address this challenge, de Palazzo et. al. developed a bispecific mAb from the somatic fusion of anti-CA 19–9 (1116NS-19-9) and anti-α-human FcγR III (3G8) antibodies.[69] After screening, cl.158 clone was chosen due to excellent binding to both SW 1116 cells and purified polymorphonuclear leukocytes. The new bispecific antibody cl.158 caused lysis of human colorectal carcinoma cell SW948 by human peripheral blood lymphocytes in low concentrations of 25 pg/ml–250 ng/ml, while its parental 3G8 and 1116NS-19-9 were unable to do so. Thus, combining anti-CA 19–9 antibodies with other targeting mechanisms, such as bispecific antibodies, enhances immune response efficacy against cancer cells.

It is known that TACAs generally are B cell antigens, which do not directly elicit T cell responses. To elicit a T cell response against tumor by anti-TACA antibodies, an innovative platform is through the design of bispecific antibodies called bispecific T cell engager (BiTE) that can bind to both the target antigen and a T cell marker such as CD3. An anti-CA 19–9 BiTE was developed by Nishimura and coworkers.[70] They linked the Fab domain of the anti-CA 19–9 mAb KM231 with that of an anti-CD3 mAb. The resulting bispecific antibody led to a great augmentation of cytotoxicity of CD3+ T cells against tumor cells, while the T cells alone only had marginal activity in killing tumor cells. Furthermore, the combination of CD4+ T cell and the anti-CA 19–9 BiTE drastically reduced tumor growth in a mouse model, while administration of the antibody or T cell alone was much less effective. These results highlight the potential of CA 19–9 targeting for tumor immunotherapy.

As a T cell independent B cell antigen, CA 19–9 does not directly elicit a cellular immune response. However, anti-CA 19–9 antibodies can be grafted to immune cells such as T cells to bestow the T cells with the abilities to recognize CA 19–9. This new type of cells, termed as chimeric antigen receptor (CAR) T cells, can directly recognize CA 19–9-positive cancer cells. Sadelain and coworkers engineered cytotoxic T cells to express 5B1 scFv on cell surface.[71] Such CA 19–9 CAR T cells were able to selectively kill CA 19–9-positive tumor cells, but spared CA 19–9-negative cells demonstrating the selectivity of such CAR T cells. To address the issue of tumor heterogeneity where not all tumor cells express the CA 19–9 antigen, tumor cells were exposed to low-dose radiation. Interestingly, the CA 19–9 targeting CAR T cells were able to eliminate the radiated CA 19–9-negative tumor cells as well presumably due to epitope spreading. These findings enhance the potential for applying CAR T therapy to heterogeneous solid tumors. In the clinical trial of a human patient with this CAR T cell,[71] while the combination of CAR T with low dose radiation reduced much of the tumor burden one month after the treatment, the tumor rebounded in two months suggesting further advances are needed to achieve a sustained therapeutic response.

The heterogeneity of tumor cells presents significant challenges for immunotherapy as the variants lacking the target antigen may escape the immune attack. One approach to reduce tumor escape is to simultaneously target multiple antigens. To accomplish this, Morimoto and Inouye developed a bispecific antibody against two cancer antigens, i.e., CA 19–9 and CEA.[72] To accomplish this, an anti-CA 19–9 IgM SA23.2 and an anti-CEA IgM 8CA10 were obtained, which were digested by pepsin to produce Fab′-type fragments. The two fragments were then chemically coupled with each other to form the heterodimeric bispecific antibody (Figure 5). The newly generated bispecific antibody retained the affinities with CA 19–9 and CEA. However, the anti-cancer activities of this bispecific antibody were not reported.

Antibody Tumor Inhibition Activity in Preclinical Study

With the binding affinity and specificity of anti-CA 19–9 mAbs established, their utility alone or in combination with other cancer treatment strategies has been investigated in preclinical studies using mouse tumor models *in vivo*. In an *in vivo* study to evaluate the anti-tumor activity of LC44 developed by the Li group,[25] SW 1116 human colon cancer cells, were inoculated into SCID mice pre-injected with human peripheral blood lymphocytes. After two days, mice were administered LC44, an isotype matched control antibody that did not bind CA 19–9, or phosphate buffered saline (PBS). LC44 treatment significantly increased mouse's survival from tumor challenge. Interestingly, despite the T cell apoptosis induction activity observed *in vitro* with CA 19–9, co-administering free CA 19–9 with LC44 in tumor bearing mice did not adversely influence mouse survival at the concentration investigated.

After demonstrating the CDC and ADCC activities of 5B1 in the *in vitro* study, Sawada et. al. investigated the antitumor activity of this mAb in a mouse model using Colo205-Luc tumor cells.[64] SCID mice were injected via tail vein with Colo205-Luc and received different amounts of 5B1 intraperitoneally as treatment groups and PBS as the control group. Survival rate increased to more than 2-fold, and on average more than half of the mice survived until the end of the study in treatment groups. The outcome demonstrated the tumor growth inhibitory activity of 5B1 in xenograft mouse model of colon cancer metastasis.[73] Ragupathi et. al. evaluated the antitumor activity of 5B1 in a PDAC xenograft mouse model.[73] In their study, CB17 SCID mice were grafted subcutaneously with BxPC-3, a human PDAC cell line, and then were divided into different treatment groups including 5B1 and the combination of 5B1

with gemcitabine and nab-paclitaxel, two of the most common chemotherapy drugs against PDAC. The outcome of the investigation indicated that the combination of 5B1 with chemotherapy could inhibit tumor growth by around 70–80% at day 41, which supports the potential of this mAb in combination therapy against PDAC.

Chemotherapy is one of the main methods for cancer treatment. However, due to the high toxicity and low tumor selectivity of the drugs, chemotherapy is associated with significant side effects. With the high antigen specificity, antibodies can be conjugated to drugs (antibody drug conjugate or ADC), which can selectively deliver the drug or toxic payload to cancer cells, thus minimizing damage to healthy tissues and reducing toxicity. With the overexpression of CA 19–9 on tumor cells, anti-CA 19–9 mAb was first investigated by Kaish et. al. for targeted chemotherapy.[74] An anti-CA 19–9 IgM was functionalized with *N*-succinimidyl-3-(2-pyridylthio) propionate (SPDP) followed by reduction with dithiothreitol to introduce free sulfhydryl groups to the antibody. Subsequently, the antibody was coupled to 2-pyridyldithio functionalized liposomes encapsulating Adriamycin/Doxorubicin (DXR). The antibody conjugated DXR liposomes led to significantly higher killing of CA 19–9-positive human PDAC cell line PK-1 *in vitro* as compared to cells treated with free DXR or DXR-encapsulated liposome without the antibody. Furthermore, the antibody DXR liposomes significantly reduced tumor growth in a mouse PDAC model using PK-1 with enhanced persistence of the drug delivered, highlighting the utility of CA 19–9 targeting ADC.

Application of Anti-CA 19–9 mAb in Detection of CA 19–9-Positive Malignancies

Besides their therapeutic applications, another important application of anti-CA 19–9 antibodies is in the detection of CA 19–9-positive tumors.[10–17] The levels of CA 19–9 in human sera are not a reliable biomarker for tumor detection due to the high rate of false positives since a variety of diseases other than cancer can lead to elevated amounts of CA 19–9 in circulation as well as the differential secretion of CA 19–9 from tumor with local and shed tumor phenotypes.[18] On the other hand, CA 19–9 has been approved by the FDA as an aid to manage patients with confirmed PDAC and monitor their therapeutic responses and disease progression.[9] To explore the potential of CA 19–9 as a diagnostic target, anti-CA 19–9 mAbs have been labeled and tested for imaging and detection of CA 19–9-positive tumors.

Munz et. al. prepared I-131 labeled $F(ab')_2$ fragments of anti-CA 19–9 mAb CO 29.11 and a human colon adenocarcinoma specific mAb GA 73–3 for tumor imaging.[75] *In vitro* binding study of radiolabeled antibodies with SW-948 human colorectal cancer cell line, indicated the highest radioactive signals when the two radiolabeled antibodies were combined. For *in vivo* imaging, SW-948 cells were grafted subcutaneously into nude mice, which was followed by intraperitoneal (IP) injection of labeled antibodies. Radioimmunoimaging was performed daily (for 6 days) by a large field-of-view scintillation camera from both lateral and posterior views. The data indicated the best tumor-to-tissue contrast and localization on day 4 for the group receiving the mixture of I-131 labeled mAbs.

One drawback of using mAbs in imaging is their relatively long serum half-life (10–20 days), which can lead to higher background and reduced contrast of tumors due to the presence of labeled antibodies in blood circulation. The Tomlinson group reported the development of an engineered I-124 (^{124}I) labeled anti-CA 19–9 diabody with a shorter serum half-life (4–20 h).[76] The diabody composed of only two antigen-binding Fv domains maintains the capability of bivalent binding to antigens as a full antibody (Figure 5), and yet has a much smaller size (MW ~55 kDa vs ~150 kDa for antibody). The Fv region of anti-CA 19–9 mAb 1116-NS-19-9 was expressed in NS0 murine myeloma cells, which was found to maintain its antigen-specific binding and subsequently radiolabeled with positron-emitting isotope ^{124}I. To assess the *in vivo* ability of the anti-CA 19–9 diabody for targeting tumors, nude mice carrying CA 19–9-positive cells (BxPC-3 and Capan-2) as well as CA 19–9-negative cell line (MiaPaCa-2), were injected with the radiolabeled antibody through the tail vein. The positron emission tomography[19] imaging 4 hours after injection showed fast tumor binding of anti-CA 19–9 diabody, while little blood background signals were observed 20 hours after injection supporting fast clearance from the circulation. The fast binding and high tumor-to-blood ratio for the BxPC-3 and Capan-2 xenograft preclinical models confirmed the sensitivity and specificity of the CA 19–9 diabody making it a promising candidate for clinical study. Subsequently, the anti-CA 19–9 diabody was conjugated with liposomal nanoparticles as a proof of principle for a cancer-targeted therapy delivery carrier.[77] Interestingly, despite the increased overall size of the diabody/nanoparticle conjugate, it still enabled high contrast for PET imaging of CA 19–9-positive tumor.

Using isotopes like ^{89}Zr for immuno-PET imaging enhances spatial resolution and tumor detection sensitivity compared to traditional imaging agents.[78] In comparison to ^{124}I, ^{89}Zr has a number of advantages since it has a lower positron energy resulting in a superior spatial resolution in PET, is less expensive to generate, and is simpler to purify. ^{89}Zr labeled anti-CA 19–9 mAb, ^{89}Zr-DFO-5B1, was prepared by conjugating an analog of benzyl-isothiocyanate desferrioxamine (DFO, ^{89}Zr chelator) to 5B1 mAb followed by ^{89}Zr incubation.[79] The resulting labeled antibody was administered into mice bearing a subcutaneous BxPC-3 PDAC xenograft. ^{89}Zr-DFO-5B1 enabled distinctive delineation of tumor sites by PET imaging, with tumor uptake 10-times better than a nonspecific control IgG mAb 24 hours after injection. The ability to detect PDAC by ^{89}Zr-DFO-5B1 was also evaluated in an orthotopic model with transplanted BxPC-3-luc cells in SCID mice. The detection sensitivity of ^{89}Zr-DFO-5B1 was compared to that of the FDA approved benchmark tumor imaging PET agent, fluorodeoxyglucose F18 (^{18}F-FDG). ^{89}Zr-DFO-5B1 was found to generate more than six times higher contrast in tumor tissues vs ^{18}F-FDG. Besides PDAC, the utilities of ^{89}Zr-DFO-5B1 to detect CA 19–9-positive small cell lung, colon, and bladder cancers were investigated in mouse

xenograft models using DMS79, Colo205, and HT1197 cells respectively.[79,80] In all these models, tumor was readily detected by PET in high contrast with minimal to no background uptake in normal tissues 48 hours after injection. The diagnostic sensitivity enabled by ^{89}Zr-DFO-5B1 was also compared to the common clinical test by measuring CA 19–9 levels in sera of tumor bearing mice, which were not detected despite the presence of tumor, thus highlighting the advantage of ^{89}Zr-DFO-5B1.

One potential drawback of targeting CA 19–9 for PET imaging is that CA 19–9 can be present as both a local and a circulating antigen, found not only on tumor sites but also in the bloodstream. Binding of ^{89}Zr-DFO-5B1 to circulating CA 19–9 or the low levels of CA 19–9 in normal tissues can lead to radiation exposure of normal cells, which can be a significant concern if repeated imaging procedures are necessary. In a subcutaneous Capan-2 PDAC xenograft model, biodistribution and PET imaging studies with ^{89}Zr-DFO-5B1 showed high levels of tracer in the liver, spleen, and lymph nodes of mice.[81] To reduce the accumulation of the labeled antibody in normal tissues, a pre-targeting strategy was developed when unlabeled 5B1 was administered first to partially block the antigen. This was followed by the administration of ^{89}Zr-DFO-5B1. After optimizing time intervals between injections, the PET image contrast of tumor site was significantly enhanced with lower amounts of signals from normal organs such as liver and spleen demonstrating the advantage of the preloading strategy.[81]

Pre-targeting strategies can take advantage of bio-orthogonal reactions to minimize radiation-related side effects in radionuclide imaging. This process includes 2 steps. First, a targeting agent such as a tagged mAb with high affinity towards the tumor cells was administered, which was followed by administration of radionucleotide moieties with high reactivity towards the tag on the tumor bound antibody, thus introducing the radionucleotide on the target cells. This approach has been applied to immuno-radionucleotides targeting the CA 19–9 antigen. In this study,[82] anti-CA 19–9 mAb 5B1 was modified with trans-cyclooctene (TCO) (Scheme 4). Concurrently, ^{64}Cu radioligands containing tetrazine (Tz) tags, ^{64}Cu-NOTA-PEG$_7$-Tz, and ^{64}Cu-NOTA–Tz, were also synthesized. The 5B1-TCO was administered first to CA 19–9-positive tumor-bearing mice. Following an accumulation period when the free 5B1-TCO was cleared from the blood stream, the Tz tagged radioligand was injected. TCO would react highly specifically with Tz through the bioorthogonal inverse electron demand Diels–Alder reaction between TCO and Tz *in vivo*, thus labeling 5B1-TCO bound cells with a ^{64}Cu radioligand. With the smaller molecular weight of the free ^{64}Cu radioligand, it can be cleared rapidly from the blood stream, thus lowering the background and enabling tumor detection with high contrast by PET.

Besides ^{64}Cu-based radioligand, this innovative pre-targeting method has been investigated for ^{177}Lu radioligand using 5B1-TCO as the preloading agent.[83] The administration of ^{177}Lu-DOTA-PEG$_7$-Tz, 72 hours after 5B1-TCO administration confirmed high uptake and prolonged retention of radioactivity in PDAC tissues as well as rapid clearance from non-target tissues, which led to notably high tumor-to-normal tissue ratios. Besides enabling PET imaging and diagnosis of tumor detection, it was advantageous that ^{177}Lu radionucleotide could also inhibit tumor growth, presenting an attractive theranostic application of this 2-part bait-and-chase radioligand system.

In addition to PET imaging with radionucleotide-labeled anti-CA 19–9 mAbs, the application of fluorescence-labeled anti-CA 19–9 mAbs has been reported for both *in vitro* and *in vivo* studies.[84] Compared to PET, fluorescence imaging also has high sensitivity without the safety concern stemming from

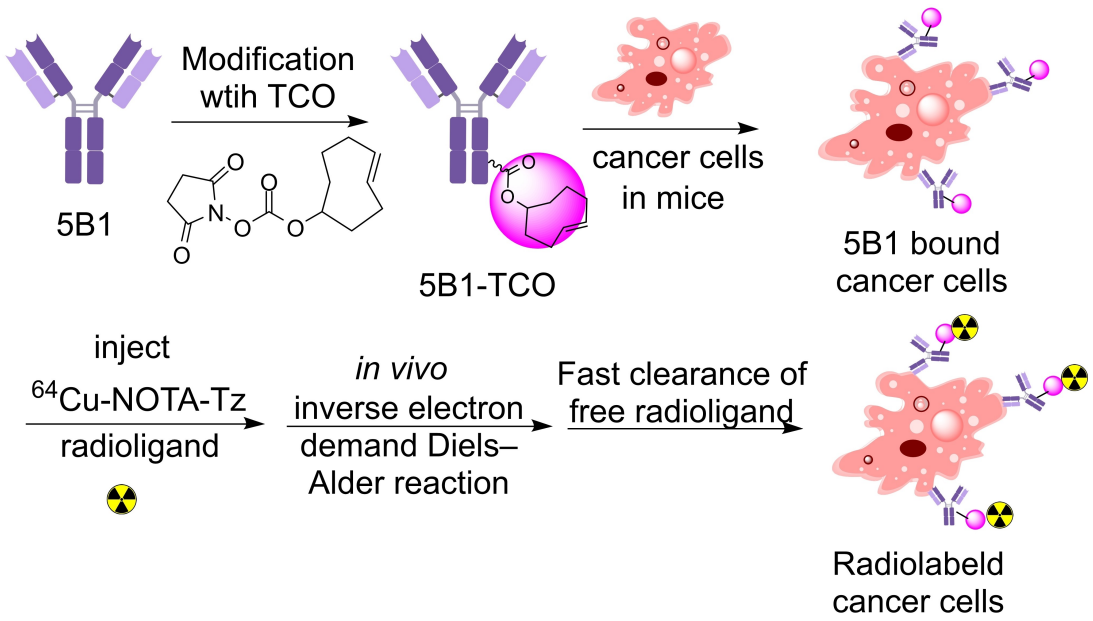

Scheme 4. Schematic demonstration of two-step pre-targeting strategy taking advantage of the bio-orthogonal reaction to selectively label tumor cells with ^{64}Cu radioligands.

the usage of radioactive nuclei in PET. The Bouvet group utilized AlexaFluor 488 labeled anti-CA 19–9 mAb to monitor the expression of CA 19–9 on a wide range of human PDAC cell lines through fluorescence imaging.[84] A variety of tumor models were investigated including subcutaneous tumor xenograft, orthotopic tumor implantation, and metastatic tumor models. Following intravenous injection of the fluorescently labeled anti-CA 19–9 mAb, the primary tumor was clearly visible via laparotomy, as were small metastatic implants in the liver and spleen and on the peritoneum. The tumor implants were challenging to detect using standard bright-field imaging techniques, but gave clear fluorescence signals under LED light irradiation, highlighting its potential for image guided surgical resection of tumor.

One of the drawbacks of fluorophore such as Alexa 488 is that Alexa 488 emits light in the visible range, which can only penetrate tissues in limited depth. In order to enhance the depth of tissue penetration, Near-infrared fluorescence (NIRF) imaging agents, IRDye650 and IRDye800CW, were conjugated to 5B1 to produce 5B1-FL650 and 5B1-FL800 respectively via NHS ester chemistry.[85] The *in vitro* binding of dye-conjugated antibodies to BxPC-3 was determined with fluorescence microscopy. The *in vivo* NIRF fluorescence imaging in both subcutaneous and orthotopic PDAC xenograft models demonstrated the potential of 5B1 in detecting pancreatic tumors for example as a NIRF-guided resection and demarcation of tumor margins.

After achieving strong results with both PET and NIRF imaging modalities, the Lewis group designed a site-specific strategy to preparing multi-modal imaging agents by conjugating PET and NIRF imaging agents to Fc domains of 5B1.[85] Rather than coupling the contrast agent with lysine residues, of which the precise locations are difficult to control, they developed a site-specific approach by remodeling the glycan chains on the mAb (Figure 6a). The galactose residues at the non-reducing end of N-glycans on heavy chains of 5B1 were first trimmed with β-1,4-galactosidase, and subsequently an azide-bearing galactose (GalNAz) was installed as catalyzed by a promiscuous galactosyltransferase GalT(Y289 L). A NIR fluorophore[65] or DFO ($^{89}Zr^{4+}$ chelator) modified with the dibenzocyclooctyne (DIBO) moiety was conjugated with the GalNAz residues site specifically (ss) via the strain promoted alkyne-azide cycloaddition reaction leading to three different immunoconjugates, ^{ss}DFO-5B1, ^{ss}FL-5B1, and ^{ss}dual-5B1 with both DFO and fluorophore. *In vitro* binding comparison of the binding between site-specifically modified immunoconjugates, $^{89}Zr^{ss}$DFO-5B1 and $^{89}Zr^{ss}$dual-5B1 to BxPC-3 pancreatic cells, with the non-site specifically labeled conjugate ^{89}Zr-DFO-5B1, indicated higher immunoreactivity for $^{89}Zr^{ss}$DFO-5B1 and $^{89}Zr^{ss}$dual-5B1. Thus, this heavy chain site-specific conjugation design is promising for antibody conjugation without interfering with the specific binding to the antigen. The *in vivo* PET and NIRF imaging evaluation of each construct in subcutaneous CA 19–9-positive, BxPC-3, and CA 19–9-negative, MiaPaCa-2, xenograft PDAC models revealed excellent uptake and contrast in CA 19–9-positive tumors with negligible nonspecific uptake in CA 19–9-negative tumors. The ^{89}Zr-^{ss}dual-5B1 was further investigated in an orthotopic murine PDAC model using Suit-2 cells, which enabled sensitive detection of cancer metastases and mapping of involved sentinel lymph nodes via tandem PET/CT and NIRF imaging (Figures 6b and c). Furthermore, NIRF imaging aided in the localization of several lymph nodes to which cancer metastasized (Figure 6c). The fluorescence signals could direct the surgical removal of the tumor containing sentinel lymph nodes with the remaining lymph nodes as well as the primary tumor shown (Figure 6d). Interestingly, NIRF imaging enabled the detection of multiple micrometastases that were not delineated in the PET/CT scans, highlighting the advantage of multi-modality imaging.

Clinical Trials

Human studies for imaging as a tumor detection tool by taking advantage of labeled anti-CA 19–9 antibodies started in 1994 in

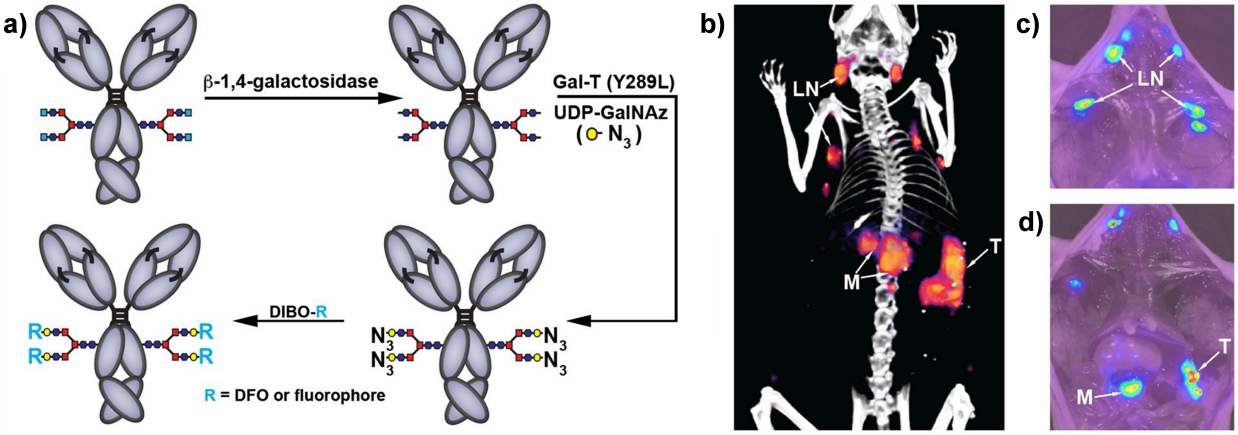

Figure 6. a) Schematic demonstration of enzymatic remodeling of glycans on mAb, which enabled site specific introduction of radiolabels into the mAb. b) PET/CT imaging of mice with primary and metastatic PDAC, showing high uptake of the tracer in the primary tumor, a metastatic site, and sentinel lymph nodes (LN, lymph nodes; M, metastasis; T, tumor). NIRF imaging of c) the sentinel lymph nodes; and d) after surgical removal of the lymph nodes demonstrating the potential of the ^{89}Zr-^{ss}dual-5B1 for image guided surgery. (Adapted from ref.[85] Copyright permission from the National Academy of Sciences, USA).

Japan when Naruki et. al. evaluated the efficiency of ^{131}I-labeled IgG F(ab')$_2$ fragments of mouse anti-CEA and CA 19–9 monoclonal antibodies (IMACIS-1) for cancer detection in patients with gastrointestinal neoplasm and liver metastases.[86] They found that metastatic cancer in liver could be effectively detected with IMACIS-1 by radioimmunoscintigraphy (RIS). In the same year, Boilleau et. al. compared the sensitivity and specificity of anatomical computed tomography (CT) versus ^{131}I gamma emission RIS using the same IMACIS-1 antibody cocktail to detect lung cancer lymph node metastases.[87] A controlled, blind, prospective study was performed on 17 patients, but two were excluded due to thyroid uptake of iodine. The evidence indicated that all primary tumors were detected by RIS. Comparing histological, CT-scan, and RIS results illustrated higher specificity for RIS but higher sensitivity for CT-scan in detecting lymph node metastasis in patients with lung cancer.

More recent clinical trials have focused on using the human 5B1 mAb with a radiotracer. In 2019, the phase I dose-escalating clinical trial (NCT02687230) was conducted for Immuno-radionucleotide, ^{89}Zr-DFO-5B1, known as MVT-2163. Twelve patients with CA 19–9-positive primary pancreatic tumors and metastatic disease received MVT-2163 and underwent PET/CT scanning for 7 days. The pre-targeting strategy of applying unlabeled 5B1 mAb prior to radiolabeled 5B1 was also adapted. The pharmacokinetics, biodistribution, radiation dosimetry, and tumor targeting of MVT-2163 were evaluated. According to the PET imaging results, the MVT-2163 tumor uptake was high and increased over time, the metastasis lesions were visualized with high contrast, and the side effects caused by MVT-2163 were under control, which makes it a safe and promising agent in PET imaging for early diagnosis of CA 19–9-positive malignancies.[88] A second diagnosis PET imaging phase 1 clinical trial (NCT05737615) started in 2023 investigating the safe doses of 5B1-TCO and ^{64}Cu–Tz-SarAr, a ^{64}Cu radioligand. This study is in the recruiting stage, taking advantage of pre-targeting strategy in PET imaging for detecting CA 19–9-positive cancerous cells and sites. Another phase 1 study (NCT03118349) was reported evaluating the safety and dosimetry as well as determining the maximum tolerated dose for ^{177}Lu-5B1 in combination with 5B1 for patients with CA 19–9-positive pancreatic ductal adenocarcinoma or other cancers (N = 24). This study was terminated in 2018, but the results have not been published.

Besides imaging applications, mAb 5B1 is currently used in an ongoing open-label, non-randomized, multicenter, dose escalation/expansion phase I trial (NCT02672917) to evaluate its therapeutic effect. The maximum tolerated dose and the recommended phase 2 dose (RP2D) for 5B1 as monotherapy and in combination with chemotherapy (mFOLFIRINOX) will be defined in PDAC patients in addition to other CA 19–9-positive cancers.

One of the challenges of cancer treatment is recurrence after tumor resection. Numerous studies indicate that removing tumors by surgery may lead to micrometastases for various reasons: 1) surgery can increase the number of cancer cells circulating in the blood; 2) stress and inflammatory signaling, as a consequence of surgery, can activate remote disseminated cancerous cells to grow; and 3) chemotherapy as an interrupting factor in the wound healing process is typically held 2–4 weeks prior to surgery, and not restarted until the patient has recovered postoperatively, up to 12 weeks. Therefore, to address the need for a safe drug to be administered immediately pre- and post-surgery, a prospective phase II study was conducted (NCT03801915).[89] The goal of this study was to evaluate the efficacy and safety of 5B1 administration within days pre- and post-surgery for patients with metastatic colorectal cancer (N = 24), cholangiocarcinoma (N = 24), and PDAC (N = 23) with high level of CA 19–9 in their blood. The perioperative use of 5B1 has the potential to reduce recurrence rates and prolong survival after resection, providing an extra tool for cancer treatment. This study was completed in March 2023, and the result has not been published yet.

A summary of clinical trials on CA 19–9 based antibodies is presented in Table 2.

Conclusions and Future Perspective

Since the discovery of carbohydrate antigen CA 19–9, numerous studies have been conducted. This review begins with discussion on diverse synthesis strategies for CA 19–9 and their applications in CA 19–9-based vaccines. Additionally, it emphasizes the development of related antibodies and their variants, which were evaluated for their therapeutic and diagnosis/imaging applications to treat and detect CA 19–9-positive malignancies.

With the development of the fully human anti-CA 19–9 mAb 5B1, it has become the focal point of many preclinical studies and clinical trials. A variety of PET tracer-labeled 5B1 constructs have been investigated using different positron-emitted radionucleotides such as ^{64}Cu and ^{89}Zr. However, concerns arise regarding extensive usage of radionucleotide-5B1 conjugation in PET imaging due to the risk of normal cells exposure to radiation. Innovative strategies such as blocking with unconjugated 5B1 as well as two-step labeling via biorthogonal reactions of radioligands in pre-targeted approaches can offer solutions to this challenge. To enhance image contrast, antibody fragments have been developed to shorten serum half-life and enhance clearance rate, which could minimize radiation exposure to normal tissues.

Considering the aggressive nature of PDAC, while most studies on CA 19–9-based constructs have been focused on imaging and detection of CA 19–9-positive tumor, the applications of CA 19–9 targeting strategies must be explored for therapy in order to enhance the survival of cancer patients. For cancer such as PDAC where the tumor microenvironment is highly fibrotic,[90] antibodies with their large sizes may have limited depth of penetration into the tumor tissues. Smaller constructs such as nanobodies can be appealing. The biodistribution, pharmacokinetics, and effector eliciting abilities of the antibodies will need to be carefully optimized through antibody engineering. In parallel, effective CA 19–9 targeting vaccines should be continuously developed as successful vaccines can induce high affinity and long-lasting antibodies to provide

Table 2. A summary of the reported CA 19–9 based antibody clinical trials.

NCT Number	Study Title	Study Status	Conditions
NCT03801915	Perioperative MVT-5873, a Fully Human Monoclonal Antibody Against a CA 19–9 Epitope, for Operable CA 19–9 Producing Pancreatic Cancers, Cholangiocarcinomas, and Metastatic Colorectal Cancers	Completed	Colon Cancer, Pancreatic Cancer, Cholangiocarcinoma, Metastatic Colon Carcinoma, Liver Metastasis
NCT04883775	Study of a New Technique for Imaging Pancreatic Cancer	Active not recruiting	Pancreatic Cancer, Tumors That Express CA 19–9
NCT03118349	Study of ^{177}Lu Human Monoclonal Antibody 5B1 (MVT-1075) in Combination with a Blocking Dose of MVT-5873 as Radioimmunotherapy	Terminated	Pancreatic Carcinoma, Tumors That Express CA 19–9
NCT02672917	Study of HuMab-5B1 (MVT-5873) in Subjects With Pancreatic Cancer or Other Cancer Antigen 19–9 (CA 19–9) Positive Malignancies	Recruiting	Pancreatic Cancer
NCT02687230	Phase 1 Imaging Study of ^{89}Zr-DFO-HuMab-5B1 With HuMab-5B1	Terminated	Pancreatic Carcinoma, Tumors That Express CA 19–9
NCT05737615	PET Imaging Using ^{64}Cu–Tz-SarAr and hu5B1-TCO in People With Pancreatic, Colorectal, Bladder Cancer or Cancers With Elevated CA19.9	Recruiting	Pancreatic Cancer, Pancreatic Ductal Adenocarcinoma, Metastatic Pancreatic Ductal Adenocarcinoma, Primary Pancreatic Ductal Adenocarcinoma, Metastatic Pancreatic Cancer

long-term immune surveillance against tumors. This can potentially protect patients from metastatic cancer and reduce the rate of relapse. Since CA 19–9 has low inherent immunogenicity, innovative methods are needed to design powerful vaccine constructs. The Qβ-CA 19–9 construct provides a promising lead as a vaccine, which will need to be further optimized and evaluated for its efficacy in clinical trials.

In order to improve therapeutic efficacy, anti-CA 19–9 antibody-based ADCs can be very powerful to selectively deliver cytotoxic agents to tumor sites. Highly toxic drugs beyond DXR can be conjugated to anti-CA 19–9 antibodies. Constructs such as nanobodies and diabodies with smaller sizes and potentially enhanced tissue penetration can be attractive platforms for ADC. Innovative chemistry will need to be developed to conjugate the drugs through a suitable linker to the antibodies without adversely affecting CA 19–9 epitope binding. Furthermore, cleavage chemistry can be designed to selectively release the drug upon reaching the tumor site to reduce toxicities to normal tissues. Beyond ADCs, anti-CA 19–9 antibodies can also be adapted for cellular therapy against cancer. Newer generations of anti-CA 19–9 BiTE and CAR–T cells can be developed to initiate T cell attack on cancer cells to enhance anti-tumor efficacy.

Overall, this review highlights the potential of targeting CA 19–9 for the diagnosis, detection, and treatment of cancers. The ongoing preclinical and clinical development focusing on varying configurations of anti-CA 19–9 antibodies and associated products hold great promise for improving outcomes for patients with CA 19–9-positive cancers.

Abbreviations

A/I ratio	activating versus inhibitory ratio
ADC	antibody drug conjugates
ADCC	antibody dependent cell mediated cytotoxicity
ADCP	antibody-dependent cellular phagocytosis
Alloc	allyloxycarbonate
ATP	adenosine 5′- triphosphate
BCR	B-cell receptors
BfFKP	*Bacteroides fragilis* strain NCTC9343 bifunctional L-fucokinase/GDP-fucose pyrophosphorylase
BiGalHexNAcP	*Bifidobacterium infantis* D-galactosyl-b1–3-N-acetyl-D-hexosamine phosphorylase
Bn	benzyl
CA 19–9	carbohydrate antigen 19–9
CAR-T cell	chimeric antigen receptor T cell
CD40 L	CD40 ligand
CDC	Complement-dependent cytotoxicity
CDR	complementary-determining regions
CHO	Chinese hamster ovary
CMP-Neu5Ac	cytidine-5′-monophospho-*N*-acetylneuraminic acid
CRC	colorectal cancer cell
Cst-I	*Campylobacter jejuni* α2,3-sialyltransferase I
CT	computed tomography
CTP	cytidine 5′-triphosphate
DIBO	dibenzocyclooctyne
DXR	Doxorubicin
EGFR	epidermal growth factor receptor
ELISA	enzyme-linked immunosorbent assay
Fab	fragment antigen-binding
FACS	fluorescence-activated cell sorting
Fc	crystallizable region
FDA	food and drug administration
FL	fluorophore
Fuc	fucose
FUT3	fucosyl transferase 3

Fv	variable region
Gal	galactose
GalNAz	*N*-azido galactose
GDP-Fuc	guanosine-5′-diphosphate-fucose
GlcNAc	*N*-acetyl glucosamine
GTP	guanosine 5′-triphosphate
Hp3/4FT	*Helicobacter pylori* α1-3/4-fucosyltransferase
IP injection	intraperitoneal injection
KLH	keyhole limpet hemocyanin
LacNAc	*N*-acetyllactosamine
Le^a	Lewis A
mAb	monoclonal antibody
ManNAc	*N*-acetyl mannosamine
Neu5Ac	*N*-acetylneuraminic acid
NIRF	near-infrared fluorescence
NmCSS	*Neisseria meningitidis* CMP-sialic acid synthetase
OPME	one-pot multienzyme
PBS	phosphate buffered saline
PDAC	pancreatic ductal adenocarcinoma
PMBC	peripheral blood mononuclear cells
PmNanA	Pasteurella multocida sialic acid aldolase
PmPpA	*Pasteurella multocida* inorganic pyrophosphatase
PmST1_M144D	*Pasteurella multocida* α2-3-sialyltransferase 1 M144D mutant
RIS	radioimmunoscintigraphy
RP2D	recommended phase 2 dose
scFv	single chain fragment variable region
sLe^a	sialyl Lewis A
SPDP	*N*-succinimidyl-3-(2-pyridylthio) propionate
SpGalK	*Streptococcus pneumoniae* galactokinase
SPR	surface plasmon resonance
TACA	tumor-associated carbohydrate antigens
TCO	trans-cyclooctene
TCR	T cell receptor
TFA	trifluoroacetate
T_h	helper T cell
TMSOTf	trimethylsilyl trifluoromethanesulfonate
Type I LacNAc	Galβ1–3GlcNAc
Tz	tetrazine
V_H	variable heavy chain
V_L	variable light chain
VLP	virus-like particle
YSD: yeast surface display	

Acknowledgements

We are grateful to the National Cancer Institute, National Institutes of Health (Grant R01 CA225105 to X.H. and R42GM143998 to X.C.), Henry-Ford Health-Michigan State University to X.H. and H.C., and MSU Tetrad Interdisciplinary Funding Program to L. Q., X.H., L. S. for financial support of our work.

Conflict of Interests

Xuefei Huang is the founder of Iaso Therapeutics Inc., which is dedicated to the development of next generation of vaccines. Xi Chen is collaborating with Integrated Micro-Chromatography System (IMCS) on a current National Institutes of Health (NIH) grant (grant number: R42GM143998) focusing on developing reagents, enzymes, and methods that are ready for commercialization to allow low-cost access to sialoglycans of high demands and their underlying asialoglycans by the broad scientific community. IMCS played no role in the design, execution, interpretation, or publication of this study.

Keywords: antibodies · CA 19-9 · cancer · synthesis · vaccines

[1] A. Varki, *Glycobiol.* **2016**, *27*, 3–49.
[2] R. A. Dwek, *Chem. Rev.* **1996**, *96*, 683–720.
[3] S. R. Stowell, T. Ju, R. D. Cummings, *Annu. Rev. Pathol.* **2015**, *10*, 473–510.
[4] C. Reily, T. J. Stewart, M. B. Renfrow, J. Novak, *Nat. Rev. Nephrol.* **2019**, *15*, 346–366.
[5] J. C. Lumibao, J. R. Tremblay, J. Hsu, D. D. Engle, *J. Exp. Med.* **2022**, *219*, e20211505.
[6] S. J. Danishefsky, J. R. Allen, *Angew. Chem. Int. Ed.* **2000**, *39*, 836–863 and references cited therein.
[7] Z. Yin, X. Huang, *J. Carbohydr. Chem.* **2012**, *31*, 143–186 and references cited therein.
[8] J. Munkley, *Oncol. Lett.* **2019**, *17*, 2569–2575.
[9] T. Lee, T. Z. J. Teng, V. G. Shelat, *World J. Gastrointest. Surg.* **2020**, *12*, 468–490.
[10] P. A. Fetsch, A. Abati, Y. M. Hijazi, *Cancer Cytopathol.* **1998**, *84*, 101–108.
[11] Y. Ikeda, M. Mori, K. Kajiyama, Y. Haraguchi, O. Sasaki, K. Sugimachi, *J. Surg. Oncol.* **1996**, *62*, 171–176.
[12] Y. Ikeda, M. Mori, T. Kamakura, M. Saku, K. Sugimachi, *Eur. J. Surg. Oncol.* **1995**, *21*, 168–175.
[13] T. Iwamura, T. Katsuki, K. Ide, *Jpn. J. Cancer Res.* **1987**, *78*, 54–62.
[14] K. Makino, T. Ogata, H. Miyake, S. Habu, T. Nishimura, *Jpn. J. Cancer Res.* **1994**, *85*, 887–891.
[15] T. Nakagoe, K. Fukushima, A. Nanashima, T. Sawai, T. Tsuji, M. Jibiki, H. Yamaguchi, T. Yasutake, H. Ayabe, T. Matuo, *Can. J. Gastroenterol. Hepatol.* **2000**, *14*, 753–760.
[16] T. Rasmuson, G. Björk, L. Damber, S. Holm, L. Jacobsson, A. Jeppsson, T. Stigbrand, G. Westman, *Acta Radiol. Oncol.* **1983**, *22*, 209–214.
[17] R. A. Soslow, R. V. Rouse, M. R. Hendrickson, E. G. Silva, T. A. Longacre, *Int. J. Gynecol. Pathol.* **1996**, *15*, 257–265.
[18] A. Chan, I. Prassas, A. Dimitromanolakis, R. E. Brand, S. Serra, E. P. Diamandis, I. M. Blasutig, *Clin. Cancer Res.* **2014**, *20*, 5787–5795.
[19] H. Koprowski, Z. Steplewski, K. Mitchell, M. Herlyn, D. Herlyn, P. Fuhrer, *Somat. Cell Genet.* **1979**, *5*, 957–971.
[20] O. Insug, L. Otvos Jr, T. Kieber-Emmons, M. Blaszczyk-Thurin, *Peptides* **2002**, *23*, 999–1010.
[21] K. Iwai, H. Ishikura, M. Kaji, H. Sugiura, A. Ishizu, C. Takahashi, H. Kato, T. Tanabe, T. Yoshtki, *Int. J. Cancer* **1993**, *54*, 972–977.
[22] U. Srinivas, P. Påhlsson, A. Lundblad, *Scand. J. Immunol.* **1996**, *44*, 197–203.
[23] A. Takada, K. Ohmori, N. Takahashi, K. Tsuyuoka, A. Yago, K. Zenita, A. Hasegawa, R. Kannagi, *Biochem. Biophys. Res. Commun.* **1991**, *179*, 713–719.
[24] D. D. Engle, H. Tiriac, K. D. Rivera, A. Pommier, S. Whalen, T. E. Oni, B. Alagesan, E. J. Lee, M. A. Yao, M. S. Lucito, *Science* **2019**, *364*, 1156–1162.
[25] Z. Li, X. Liu, Y. Wan, W. Wang, J. Ma, *Cancer Biother. Radiopharm.* **2007**, *22*, 597–606.
[26] U. K. Ballehaninna, R. S. Chamberlain, *Indian J. Surg. Oncol.* **2011**, *2*, 88–100.

[27] S. Salleh, A. Thyagarajan, R. P. Sahu, *J. Cancer Metastasis Treat.* **2020**, *6*, 31. DOI: 10.20517/22394-24722.22020.20570.
[28] B. Zhao, B. Zhao, F. Chen, *Eur. J. Gastroenterol. Hepatol.* **2022**, *34*, 891–904.
[29] G. Luo, K. Jin, S. Deng, H. Cheng, Z. Fan, Y. Gong, Y. Qian, Q. Huang, Q. Ni, C. Liu, X. Yu, *Biochim. Biophys. Acta Rev. Cancer* **2021**, *1875*, 188409.
[30] L. E. Kane, G. S. Mellotte, E. Mylod, R. M. O'Brien, F. O'Connell, C. E. Buckley, J. Arlow, K. Nguyen, D. Mockler, A. D. Meade, B. M. Ryan, S. G. Maher, *Cancer Res. Commun.* **2022**, *2*, 1229–1243.
[31] X. Zhou, *Int. J. Biol. Sci.* **2022**, *37*, 81–89.
[32] T. Yue, K. Partyka, K. A. Maupin, M. Hurley, P. Andrews, K. Kaul, A. J. Moser, H. Zeh, R. E. Brand, B. B. Haab, *Proteomics* **2011**, *11*, 3665–3674.
[33] J. L. Magnani, B. Nilsson, M. Brockhaus, D. Zopf, Z. Steplewski, H. Koprowski, V. Ginsburg, *J. Biol. Chem.* **1982**, *257*, 14365–14369.
[34] G. Hansson, D. Zopf, *J. Biol. Chem.* **1985**, *260*, 9388–9392.
[35] M. Kiso, H. Furui, K. Ando, H. Ishida, A. Hasegawa, *Bioorg. Med. Chem. Lett.* **1994**, *2*, 1295–1308.
[36] K. Peilstoecker, H. Kunz, *Synlett* **2000**, *2000*, 0820–0822.
[37] G. Ragupathi, P. Damani, G. Srivastava, O. Srivastava, S. J. Sucheck, Y. Ichikawa, P. O. Livingston, *Cancer Immunol. Immunother.* **2009**, *58*, 1397–1405.
[38] Z. Rashidijahanabad, S. Ramadan, N. A. O'Brien, A. Nakisa, S. Lang, H. Crawford, J. C. Gildersleeve, X. Huang, *Angew. Chem. Int. Ed.* **2023**, *62*, e202309744.
[39] Y. Jiang, S. Duan, J. Li, Y. Zhao, J. Yang, *Org. Biomol. Chem.* **2024**, *22*, 5776–5782.
[40] J. Weinstein, U. de Souza-e-Silva, J. Paulson, *J. Biol. Chem.* **1982**, *257*, 13835–13844.
[41] M. M. Palcic, A. P. Venot, R. M. Ratcliffe, O. Hindsgaul, *Carbohydr. Res.* **1989**, *190*, 1–11.
[42] M. Bårström, M. Bengtsson, O. Blixt, T. Norberg, *Carbohydr. Res.* **2000**, *328*, 525–531.
[43] B. Gabi, Ö. Reinhold, S. Markus, K. Frank, *Bioorg. Med. Chem. Lett.* **1998**, *8*, 755–758.
[44] Y. Makimura, H. Ishida, A. Kondo, A. Hasegawa, M. Kiso, *J. Carbohydr. Chem.* **1998**, *17*, 975–979.
[45] N. Tasnima, H. Yu, X. Yan, W. Li, A. Xiao, X. Chen, *Carbohydr. Res.* **2019**, *472*, 115–121.
[46] H. Yu, V. Thon, K. Lau, L. Cai, Y. Chen, S. Mu, Y. Li, P. G. Wang, X. Chen, *Chem. Commun.* **2010**, *46*, 7507–7509.
[47] G. Sugiarto, K. Lau, J. Qu, Y. Li, S. Lim, S. Mu, J. B. Ames, A. J. Fisher, X. Chen, *ACS Chem. Biol.* **2012**, *7*, 1232–1240.
[48] B. Acres, S. Paul, H. Haegel-Kronenberger, B. Calmels, P. Squiban, *Curr. Opin. Mol. Ther.* **2004**, *6*, 40–47.
[49] M. Saxena, S. H. van der Burg, C. J. M. Melief, N. Bhardwaj, *Nat. Rev. Cancer* **2021**, *21*, 360–378.
[50] M. A. Morse, W. R. Gwin, D. A. Mitchell, *Target. Oncol.* **2021**, *16*, 121–152.
[51] R. Elgueta, M. J. Benson, V. C. De Vries, A. Wasiuk, Y. Guo, R. J. Noelle, *Immunol. Rev.* **2009**, *229*, 152–172.
[52] A. Diab, G. Ragupathi, W. W. Scholz, K. Panageas, C. Hudis, P. O. Livingston, T. Gilewski, *J. Clin. Oncol.* **2011**, *29*, 2599–2599.
[53] S. Nooraei, H. Bahrulolum, Z. S. Hoseini, C. Katalani, A. Hajizade, A. J. Easton, G. Ahmadian, *J. Nanobiotechnol.* **2021**, *19*, 1–27.
[54] S. Sungsuwan, X. Wu, V. Shaw, H. Kavunja, H. McFall-Boegeman, Z. Rashidijahanabad, Z. Tan, S. Lang, S. T. Nick, P.-H. Lin, Z. Yin, S. Ramadan, X. Jin, X. Huang, *ACS Chem. Biol.* **2022**, *17*, 3047–3058.
[55] R.-M. Lu, Y.-C. Hwang, I.-J. Liu, C.-C. Lee, H.-Z. Tsai, H.-J. Li, H.-C. Wu, *J. Biomed. Sci.* **2020**, *27*, 1–30.
[56] R. Singh, P. Chandley, S. Rohatgi, *ImmunoHorizons* **2023**, *7*, 886–897.
[57] J. K. Liu, *Ann. Med. Surg.* **2014**, *3*, 113–116.
[58] S. Mitra, P. C. Tomar, *J. Genet. Eng. Biotechnol.* **2021**, *19*, 1–12.
[59] J. L. Magnani, M. Brockhaus, D. F. Smith, V. Ginsburg, M. Blaszczyk, K. F. Mitchell, Z. Steplewski, H. Koprowski, *Science* **1981**, *212*, 55–56.
[60] M. Herlyn, H. F. Sears, Z. Steplewski, H. Koprowski, *J. Clin. Immunol.* **1982**, *2*, 135–140.
[61] J. L. Magnani, Z. Steplewski, H. Koprowski, V. Ginsburg, *Cancer Res.* **1983**, *43*, 5489–5492.
[62] M. Herlyn, M. Blaszczyk, J. Bennicelli, H. F. Sears, C. Ernst, A. H. Ross, H. Koprowski, *J. Immunol. Methods* **1985**, *80*, 107–116.
[63] C. D. Gimmi, B. W. Morrison, B. A. Mainprice, J. G. Gribben, V. A. Boussiotis, G. J. Freeman, S. Y. Lee Park, M. Watanabe, J. Gong, D. F. Hayes, *Nat. Med.* **1996**, *2*, 1367–1370.
[64] R. Sawada, S.-M. Sun, X. Wu, F. Hong, G. Ragupathi, P. O. Livingston, W. W. Scholz, *Clin. Cancer Res.* **2011**, *17*, 1024–1032.
[65] A. Borenstein-Katz, S. Warszawski, R. Amon, M. Eilon, H. Cohen-Dvashi, S. Leviatan Ben-Arye, N. Tasnima, H. Yu, X. Chen, V. Padler-Karavani, S. J. Fleishman, R. Diskin, *J. Mol. Biol.* **2021**, *433*, 167099.
[66] R. Amon, R. Rosenfeld, S. Perlmutter, O. C. Grant, S. Yehuda, A. Borenstein-Katz, R. Alcalay, T. Marshanski, H. Yu, R. Diskin, R. J. Woods, X. Chen, V. Vered Padler-Karavani, *Cancers* **2020**, *12*, 2824.
[67] F. Nimmerjahn, J. V. Ravetch, *Science* **2005**, *310*, 1510–1512.
[68] P. Weitzenfeld, S. Bournazos, J. V. Ravetch, *J. Clin. Invest.* **2019**, *129*, 3952–3962.
[69] I. G. de Palazzo, C. Gercel-Taylor, J. Kitson, L. M. Weiner, *Cancer Res.* **1990**, *50*, 7123–7128.
[70] O. So, T. Hideo, W. Kazuhito, M. Koji, K. Soichi, H. Nobuo, H. Sonoko, N. Takashi, *Immunol. Lett.* **1995**, *44*, 35–40.
[71] C. DeSelm, M. L. Palomba, J. Yahalom, M. Hamieh, J. Eyquem, V. K. Rajasekhar, M. Sadelain, *Mol. Ther.* **2018**, *26*, 2542–2552.
[72] K. Morimoto, K. Inouye, *J. Immunol. Methods* **1999**, *224*, 43–50.
[73] G. Ragupathi, X. Wu, P. Livingston, W. Scholz, C. Kearns, P. Maffuid, *Cancer Res.* **2016**, *76*, A73–A73.
[74] S. Akaishi, M. Kobari, K. Takeda, S. Matsuno, *Tohoku J. Exp. Med.* **1995**, *175*, 29–42.
[75] D. L. Munz, A. Alavi, H. Koprowski, D. Herlyn, *J. Nucl. Med.* **1986**, *27*, 1739–1745.
[76] M. D. Girgis, V. Kenanova, T. Olafsen, K. E. McCabe, A. M. Wu, J. S. Tomlinson, *J. Surg. Res.* **2011**, *170*, 169–178.
[77] M. D. Girgis, N. Federman, M. M. Rochefort, K. E. McCabe, A. M. Wu, J. O. Nagy, C. Denny, J. S. Tomlinson, *J. Surg. Res.* **2013**, *185*, 45–55.
[78] J.-K. Yoon, B.-N. Park, E.-K. Ryu, Y.-S. An, S.-J. Lee, *Int. J. Mol. Sci.* **2020**, *21*, 4309.
[79] N. T. Viola-Villegas, S. L. Rice, S. Carlin, X. Wu, M. J. Evans, K. K. Sevak, M. Drobjnak, G. Ragupathi, R. Sawada, W. W. Scholz, *J. Nucl. Med.* **2013**, *54*, 1876–1882.
[80] F. E. Escorcia, J. M. Steckler, D. Abdel-Atti, E. W. Price, S. D. Carlin, W. W. Scholz, J. S. Lewis, J. L. Houghton, *Mol. Imaging Biol.* **2018**, *20*, 808–815.
[81] J. L. Houghton, D. Abdel-Atti, W. W. Scholz, J. S. Lewis, *Mol. Pharm.* **2017**, *14*, 908–915.
[82] J. L. Houghton, B. M. Zeglis, D. Abdel-Atti, R. Sawada, W. W. Scholz, J. S. Lewis, *J. Nucl. Med.* **2016**, *57*, 453–459.
[83] J. L. Houghton, R. Membreno, D. Abdel-Atti, K. M. Cunanan, S. Carlin, W. W. Scholz, P. B. Zanzonico, J. S. Lewis, B. M. Zeglis, *Mol. Cancer Ther.* **2017**, *16*, 124–133.
[84] M. McElroy, S. Kaushal, G. A. Luiken, M. A. Talamini, A. R. Moossa, R. M. Hoffman, M. Bouvet, *World J. Surg.* **2008**, *32*, 1057–1066.
[85] J. L. Houghton, B. M. Zeglis, D. Abdel-Atti, R. Aggeler, R. Sawada, B. J. Agnew, W. W. Scholz, J. S. Lewis, *Proc. Natl. Acad. Sci. USA* **2015**, *112*, 15850–15855.
[86] Y. Naruki, Y. Urita, Y. Miyachi, S. Otsuka, M. Noguchi, T. Kogure, Y. Sasaki, *Ann. Nucl. Med.* **1994**, *8*, 163–169.
[87] G. Boilleau, J.-L. Pujol, M. Ychou, P. Faurous, C. Marty-Ané, F.-B. Michel, P. Godard, *Lung Cancer* **1994**, *11*, 209–219.
[88] C. Lohrmann, E. M. O'Reilly, J. A. O'Donoghue, N. Pandit-Taskar, J. A. Carrasquillo, S. K. Lyashchenko, S. Ruan, R. Teng, W. Scholz, P. W. Maffuid, *Clin. Cancer Res.* **2019**, *25*, 7014–7023.
[89] S. Gupta, J. D. McDonald, R. I. Ayabe, T. M. Khan, L. A. Gamble, S. Sinha, C. Hannah, A. M. Blakely, J. L. Davis, J. M. Hernandez, *J. Gastrointest. Oncol.* **2020**, *11*, 231.
[90] L. F. Sempere, K. Powell, J. Rana, A. A. Brock, T. D. Schmittgen, *Cancer Metastasis Rev.* **2021**, *40*, 761–776.

Manuscript received: June 27, 2024
Revised manuscript received: August 30, 2024
Accepted manuscript online: September 4, 2024
Version of record online: November 8, 2024